https://doi.org/10.5194/acp-2021-870
Preprint. Discussion started: 30 November 2021

Atmospheric Chemistry and Physics Discussions

Assessment of NAAPS-RA performance in Maritime Southeast Asia during CAMP^{2}Ex

Eva-Lou Edwards[1], Jeffrey S. Reid[2], Peng Xian[2], Sharon P. Burton[3], Anthony L. Cook[3], Ewan C. Crosbie[3,4], Marta A. Fenn[3,4], Richard A. Ferrare[3], Sean W. Freeman[5], John W. Hair[3], David B. Harper[3], Chris A. Hostetler[3], Claire E. Robinson[3,4], Amy Jo Scarino[3,4], Michael A. Shook[3], G. Alexander Sokolowsky[5], Susan C. van den Heever[5], Edward L. Winstead[3,4], Sarah Woods[6], Luke D. Ziemba[3], Armin Sorooshian[1,7]

[1]Department of Chemical and Environmental Engineering, University of Arizona, Tucson, AZ, 85721, USA
[2]Marine Meteorology Division, U. S. Naval Research Laboratory, Monterey, CA, 93943, USA
[3]NASA Langley Research Center, Hampton, VA, 23681, USA
[4]Science Systems and Applications, Inc., Hampton, VA, 23666, USA
[5]Department of Atmospheric Science, Colorado State University, Fort Collins, CO, 80523, USA
[6]SPEC Inc., Boulder, CO, 80301, USA
[7]Department of Hydrology and Atmospheric Sciences, University of Arizona, Tucson, AZ, 85721, USA

[*]Corresponding author: armin@arizona.edu

https://doi.org/10.5194/acp-2021-870
Preprint. Discussion started: 30 November 2021

Atmospheric Chemistry and Physics Discussions

Abstract

Monitoring and modeling aerosol particle lifecycle in Southeast Asia (SEA) is challenged by high cloud cover, complex meteorology, and the wide range of aerosol species, sources, and transformations found throughout the region. Satellite observations are limited, and there are few in situ observations of aerosol extinction profiles, aerosol properties, and environmental conditions. Therefore, accurate aerosol model outputs are crucial for the region. This work evaluates the Navy Aerosol Analysis and Prediction System Reanalysis (NAAPS-RA) aerosol optical thickness (AOT) and light extinction products using airborne aerosol and meteorological measurements from the Cloud, Aerosol, and Monsoon Processes Philippines Experiment ($CAMP^2Ex$) in SEA. Modeled AOTs and extinction coefficients were compared to those retrieved with a High Spectral Resolution Lidar (HSRL-2). Correlations were highest for AOT in the mixed layer (AOT_{ML}; R^2 = 0.83, bias = 0.00, root mean square error [RMSE] = 0.03) compared to total AOT (R^2 = 0.68, bias = 0.01, RMSE = 0.14), although the correlations between the observations and 1° × 1° degree NAAPS-RA outputs were weaker in regions with strong gradients in aerosol properties, such as near areas of active convection. Correlations between simulated and retrieved aerosol extinction coefficients were highest from 145 – 500 m (R^2 = 0.75, bias = 0.01 km^{-1}, RMSE = 0.08 km^{-1}) and decreased with increasing altitude (R^2 = 0.69 and 0.26, bias = 0.00 and 0.00 km^{-1}, RMSE = 0.09 and 0.00 km^{-1} for 500 – 1500 m and > 1500 m, respectively), which was likely a result of the use of bulk cloud mixing parameterizations. We also investigated the role of possible relative humidity (RH) errors in extinction simulations. Despite negative biases in modeled RH (-4.9, -7.7, and -2.3% for altitudes < 500 m, 500 – 1500 m, and > 1500 m, respectively), AOT and extinction agreement with the HSRL-2 did not change significantly at any altitude when RHs from dropsondes were substituted into the model. Improvements may have been stunted due to errors in how NAAPS-RA modeled physics of particle hygroscopic growth, dry particle mass concentrations, and/or dry mass extinction efficiencies, especially when combined with AOT corrections from data assimilation. Specifically, the model overestimated the hygroscopicity of (i) smoke particles from biomass burning in the Maritime Continent (MC), and (ii) anthropogenic emissions transported from East Asia. This work provides insight into how certain environmental and microphysical properties influence AOT and extinction simulations, which can then be interpreted in the context of modeling global concentrations of particle mass and cloud condensation nuclei (CCN).

https://doi.org/10.5194/acp-2021-870
Preprint. Discussion started: 30 November 2021

Atmospheric Chemistry and Physics Discussions

1. Introduction

Southeast Asia (SEA) has long been considered one of the most susceptible locations to the repercussions of climate change (IPCC, 2013, 2007), with the Philippines considered as one of the most vulnerable in particular (Yusuf and Francisco, 2009). The Philippines is experiencing rapid urbanization, industrialization, and economic development along its extensive coastlines (Alas et al., 2018). Rising sea levels, decreased precipitation in association with the June-September southwest monsoon (SWM), prolonged droughts (Cruz et al., 2013), and increased observations of days with anomalously high rainfall (Cinco et al., 2014) all present threats to the homes, water and food security, electric needs, and livelihoods of millions of people living in this area (IPCC, 2013). Additionally, tropical cyclones and their ensuing storm surges have consistently battered the Philippines (e.g., Lagmay et al., 2015). These storms may become more severe as global temperatures increase (Sobel et al., 2016; Knutson et al., 2019). Considering all these grave threats, it is more important than ever to be able to model future environmental conditions in SEA and issue timely advisories to inhabitants of the region.

Model reanalyses are a crucial method to consistently characterize the environment, especially in a region as meteorologically complex as SEA. By combining numerical weather predictions and the best available observations, time series of a complete meteorological and compositional state can be generated for years, if not decades. Aerosol particles play a key role in the SEA regional climate and the hydrological cycle, where aerosol-cloud interactions are dictated by and, in themselves, influence atmospheric convection (e.g., Reid et al., 2012; Thornton et al., 2017; Ross et al., 2018, repectively). However, high fidelity is required to monitor and model the properties, transport pathways, and chemical evolution of aerosol particles in SEA, as well as their relationships with the complex meteorology. This has proven exceedingly difficult for multiple reasons as outlined in Reid et al. (2013). Diverse natural and anthropogenic aerosol particles with dissimilar microphysical properties converge throughout the region, including in densely populated coastal environments (e.g., Cruz et al., 2019; Hilario et al., 2020b; Kecorius et al., 2017). During the SWM, agricultural, deforestation, and peat burning crests throughout much of the Maritime Continent (MC), resulting in enormous quantities of particulate and gaseous emissions. The transport of these emissions, as well as pollution from Indonesia and Malaysia, into the Philippines and northwestern tropical Pacific (NWTP) is facilitated by southwesterly winds and reduced particle scavenging as heavy rainfall associated with the western Pacific monsoonal trough shifts to the northern hemisphere (Xian et al., 2013). At the same time, significant pollution emissions are generated from sources of varying scales, such as megacities, ships, and cook fires. Pollution from Asia, local Philippine emissions (e.g., cooking, vehicular combustion, road dust), and ship exhaust are constantly mixed with naturally emitted aerosols, such as marine particles (e.g., sea salt [Azadiaghdam et al., 2019], organic matter, and derivatives of dimethylsulfide [DMS; Stahl et al., 2020a]), dust (Cruz et al., 2019; Campbell et al., 2013), and volcanic emissions (Hilario et al., 2021). Lack of funding and various political issues have stunted efforts for routine, cohesive, and fully publically available aerosol measurements across the region (Reid et al., 2013). Satellite retrievals are frequently impinged by nearly ubiquitous cloud cover. This shortage of reliable data has resulted in a lack of quantitative knowledge of the aerosol lifecycle in this region, which has trickled down into significant model errors and uncertainty in forecasting aerosol properties and their participation in regional atmospheric processes (e.g., Adler et al., 2001; Mahmud and Ross, 2005; Dai, 2006; Sun et al., 2007; Xian et al., 2009).

For the above reasons, reanalyses are a highly attractive tool to study the environment, especially within the context of coupled systems. However, reanalyses have their own sets of

https://doi.org/10.5194/acp-2021-870
Preprint. Discussion started: 30 November 2021

Atmospheric Chemistry and Physics Discussions

uncertainties, sometimes brought about as the model attempts to reconcile observations and model physics. Although miscalculations can occur at any stage in a climate or chemical transport model (e.g., if equations modeling various atmospheric processes are based on assumptions that do not apply to the true environment), errors in fundamental parameters (e.g., RH, surface wind speed) are especially deleterious as they can propagate through subsequent calculations, leading to flawed outputs. Alternatively, error cancellation against some observable can occur when a model combines two erroneous values in a calculation. This is also problematic as it can appear the model is performing well, when in reality there are underlying issues. A prime example of this is with aerosol optical thickness (AOT), a common product produced by most aerosol models (e.g., Colarco et al., 2010; Zhu et al., 2017; Sessions et al., 2015) and reanalyses (e.g., Gelaro et al., 2017; Inness et al., 2019; Lynch et al., 2016; Randles et al., 2017; Yumimoto et al., 2017). Indeed, AOT is the principal driver for aerosol data assimilation precisely because AOT is the most available and skillful aerosol property from remote sensing. However, despite some utility for inferring information about air quality (e.g., Gupta et al., 2006), visibility (e.g., Retalis et al., 2010), and general aerosol loading (Liu et al., 2007) at a given location, the possibility for degenerate solutions (i.e., the same AOT output for a wide range of atmospheric conditions, including at the surface) can hide errors for a number of fundamental quantities needed for data interpretation (e.g., relative humidity [RH], speciated particle mass concentrations, optical properties, and vertical distribution of aerosol particles; e.g., Kaku et al., 2018).

Improving atmospheric models in SEA must occur from the ground up. Estimations for "big-picture" quantities (e.g., AOT and particle light extinction) will not progress until models are accurately quantifying both chemical and atmospheric properties. This study addresses that challenge by evaluating the Navy Aerosol Analysis and Prediction System Reanalysis (NAAPS-RA; Lynch et al., 2016) in and around the Philippines during the Cloud, Aerosol, and Monsoon Processes Philippines Experiment (CAMP^{2}Ex; Reid et al., 2021). NAAPS has been widely used and verified to understand aerosol lifecycle in SEA (Hyer and Chew, 2010; Reid et al., 2012; Reid et al., 2015; Reid et al., 2016a; Reid et al., 2016b; Xian et al., 2013; Atwood et al., 2017) and its impact on clouds (Ross et al., 2018). However, its many products have not yet been simultaneously evaluated for the region. Currently within the context of CAMP^{2}Ex, models such as NAAPS-RA are being used to define aerosol-cloud susceptibility regimes from which the larger aerosol-cloud-precipitation system can be assessed. Of primary importance is the model's ability to reproduce the marine mixed layer's aerosol properties in order to infer aerosol cloud condensation nuclei (CCN) concentrations.

In this paper, we assess model performance by comparing simulated NAAPS-RA AOT and aerosol extinction coefficients (the subsequent primary observable after AOT) to those retrieved with a High Spectral Resolution Lidar (HSRL-2; Hair et al., 2008). Given the importance of humidity and particle hygroscopicity, we subsequently replace model RH with in situ values to understand how model errors for RH affect AOT and extinction output. Then we substitute aircraft in situ observations of the hygroscopic growth parameter (γ), as well as dropsonde in situ RH values, into the model to obtain extinction coefficients when particle hygroscopic growth is quantified as accurately as possible for four case studies in the mixed layer (ML). Any remaining error in total extinction is then attributed to inaccuracies in the model representation of dry aerosol extinction (i.e., dry particle mass multiplied by dry mass extinction efficiency), which is a topic of a subsequent paper. Knowledge from this work regarding the strengths, weaknesses, and sensitivities of NAAPS-RA in SEA can better equip the modeling community to confront and revise prevalent vulnerabilities. Through synergistic efforts such as this, we inch closer towards

https://doi.org/10.5194/acp-2021-870
Preprint. Discussion started: 30 November 2021


Atmospheric Chemistry and Physics Discussions

understanding atmospheric processes in SEA and addressing projected environmental challenges ahead.

2. Methods

2.1 Field Campaign Description

The CAMP^{2}Ex field campaign examined the effect of anthropogenic and natural aerosol particles on warm and mixed-phase precipitation in SEA during the SWM and a short post-monsoon period. Some of the specific interests included (i) investigating relationships between aerosol particle properties (e.g., number concentrations, composition, spatial distribution) and shallow cumulus and congestus cloud features (e.g., optical properties, microphysical properties, their transition from shallow to deep convection), (ii) assessing how the region's meteorology both influenced and was influenced by aerosol-cloud interactions, and (iii) developing remote sensing, modeling, and technology advances to improve regional monitoring and Earth system assessment. The NASA P-3 aircraft carried out 19 research flights (RFs) between 24 August and 5 October 2019 (Table S1) equipped with a payload of instruments and remote sensors to sample the microphysical, hydrological, dynamical, thermodynamic, and radiative properties of the environment in and around the Philippines. The flight strategy consisted of (i) identifying and flying to locations with opportune meteorological conditions and/or air masses (e.g., smoke advecting from the MC, East Asian outflow, etc.), (ii) beginning with a high-altitude leg (~6 – 8 km) at the location of interest so that remote sensors (e.g., the HSRL-2) and any released dropsondes could inform of noteworthy environmental features below the aircraft, and (iii) flying to identified features to sample the relevant aerosol field, cloud properties, and environmental conditions. During CAMP^{2}Ex, the P-3 sampled diverse air masses, including long range transport of peat burning and pollution from Borneo, Asian pollution, Philippine outflow, and cleaner marine conditions (Hilario et al., 2021).

2.2 P-3 Observations and Retrievals

The P-3 carried a comprehensive package of instruments for quantifying aerosol particle properties, cloud properties, and meteorology. Here we discuss the instrument observations and retrievals relevant to this study. The HSRL-2 supplied mixed layer heights (MLHs), aerosol extinction coefficients (355, 532, 1064 nm), 355-532 nm Angstrom exponent, 532 nm depolarization ratios, and an aerosol classification product (Table 1). Dropsonde data provided vertical profiles of meteorological variables (e.g., temperature, dew point temperature, pressure, RH). Two nephelometers (TSI-3563) in parallel (Anderson and Ogren, 1998) provided the hygroscopic growth parameter (γ; 550 nm) used to calculate the hygroscopic scattering enhancement factor ($f[RH]$; Ziemba et al., 2013). An Aerodyne High-Resolution Time-of-Flight Aerosol Mass Spectrometer (AMS; Canagaratna et al., 2007; Decarlo et al., 2006) provided non-refractory, chemically resolved aerosol particle mass concentrations. The AMS was operated in 1 Hz fast mass spectral (MS) mode with final data averaged to 30-s time resolution. Finally, a fast cloud droplet probe (FCDP; SPEC Inc.; Glienke and Mei, 2020; SPEC 2013, 2019) supplied size distribution data for particles with diameters of 1.5 – 50 µm as well as liquid water content (LWC).

When the aircraft entered clouds, a counterflow virtual impactor (CVI) inlet (Shingler et al., 2012) was used to sample droplet residual particles. In cloud-free air, ambient aerosol particles were sampled continuously through an isokinetic Clarke-style shrouded solid diffuser inlet (McNaughton et al., 2007). Data used in this study were filtered to isolate those collected

https://doi.org/10.5194/acp-2021-870
Preprint. Discussion started: 30 November 2021


Atmospheric Chemistry and Physics Discussions

during isokinetic sampling and when LWC from the FCDP was below 0.02 g m^{-3}, a threshold which has been used in other works to distinguish periods spent in clouds versus clear air (Prabhakar et al., 2014; Wang et al., 2014). Throughout the following sections, we elaborate on how each of these datasets was incorporated into this study.

https://doi.org/10.5194/acp-2021-870
Preprint. Discussion started: 30 November 2021

Atmospheric Chemistry and Physics Discussions

196 **Table 1.** Summary of datasets used in this study.

Instrument/Source	Measured/Retrieved Parameter and Units	Size range	Temporal resolution	Spatial resolution	Reference
HSRL-2	Mixed layer height (m)	N/A	60 s	N/A	Scarino et al. (2014);
	Aerosol extinction coefficient (355/532/1064[a] nm) (km^{-1})			150 m (vertical) (interpolated to 15-m grid spacing)	Hair et al. (2008); Burton et al. (2018)
	Angstrom exponent (355-532 nm) (unitless)				
	Particle depolarization ratio (532 nm)		10 s	15 m	
	Aerosol classifications		60 s	150 m	Burton et al. (2013)
Vaisala RD-41 Dropsondes	Temperature (°C)	N/A	0.25 s	N/A	Vaisala (2020)
	Dew point temperature (°C)				
	Pressure (mbar)				
	Relative humidity (%)				
TSI-3563 nephelometers*	γ (550 nm) (unitless)	< 5000 nm	1 s	~100 m (horizontal)[b]	Anderson and Ogren (1998)
Aerodyne HR-ToF-AMS*	Non-refractory chemically resolved mass concentration (μg m^{-3})	60–600 nm	30 s	~3000 m (horizontal)[b]	Canagaratna et al. (2007); Decarlo et al. (2006)
SPEC Inc. FCDP	Aerosol size distribution (L^{-1})	1.5–50 μm	1 s	~100 m (horizontal)[b]	Glienke and Mei (2020); SPEC (2013, 2019)
	Liquid water content (LWC) (g m^{-3})				
Inlet flag	Flag indicating whether sampling occurred through a counterflow virtual impactor[c] (CVI) inlet or an isokinetic inlet[d] exponent (355-532 nm) (unitless)	N/A	1 s	~100 m (horizontal)[b]	Shingler et al. (2012) (CVI inlet); McNaughton et al. (2007) (isokinetic inlet);
NAAPS-RA	Speciated mass concentrations (ABF[e], smoke, dust, sea salt) (μg m^{-3})	N/A	6 h	1° × 1° (horizontal) Terrain-following coordinate system with 25 layers (vertical)	Lynch et al. (2016) and references therein
	Fine (< 1 μm) and coarse (> 1 μm) aerosol extinction coefficients (550 nm) (m^{-1})				
	Pressure layer thickness (m)				

https://doi.org/10.5194/acp-2021-870
Preprint. Discussion started: 30 November 2021

Atmospheric Chemistry and Physics Discussions

	Relative humidity (%)				

***Data were only used if they were collected during isokinetic sampling and when LWC was below 0.02 g m^{-3}.**
[a]1064 nm aerosol extinction coefficients were derived using aerosol backscatter at 1064 nm multiplied by the lidar ratio inferred from the lidar ratio measured at 532 nm and an inference of aerosol type.
[b]Based on a nominal aircraft speed of 100 m s^{-1}.
[c]Brechtel Manufacturing Inc. Model 1204 CVI
[d]University of Hawaii/Clarke-style shrouded solid diffuser inlet
[e]"ABF" stands for anthropogenic and biogenic fine.

197

https://doi.org/10.5194/acp-2021-870
Preprint. Discussion started: 30 November 2021

Atmospheric Chemistry and Physics Discussions

198 **2.3 NAAPS-RA AOT Product**

199 The U.S. Navy has long been interested in modeling the properties and behavior of
200 atmospheric aerosol particles because of their significant role in visibility, meteorology, and
201 potential interference with satellite retrievals of sea surface temperature (May et al., 1992;
202 Reynolds et al., 1989; Robock, 1989), ocean color (Gordon, 1997), and land use systems (Song
203 et al., 2001), either directly or indirectly via clouds. In response to the pressing need for an
204 aerosol reanalysis product with widespread spatial and temporal coverage, the U.S. Naval
205 Research Laboratory developed NAAPS with multiple configurations for operations, reanalyses
206 (Lynch et al., 2016 and references therein used here), and ensembles (Rubin et al., 2016). The
207 reanalysis version, NAAPS-RA, is an aerosol model intended for basic research including the
208 creation of long and consistent data records. NAAPS-RA is an offline chemical transport model
209 with a 6-hour temporal resolution, 1° × 1° spatial resolution, 25 vertical levels based on a terrain-
210 following sigma-pressure coordinate system, and meteorological fields that are driven by the
211 Navy Global Environmental Model (NAVGEM; Hogan et al., 2014). Lynch et al. (2016)
212 provides a full description of NAAPS-RA, but in short it is a chemical transport model
213 simulating the four-dimensional distribution of four aerosol species: dust, sea salt (both of which
214 are dominated by coarse mode [> 1μm] particles), open biomass burning smoke, and a combined
215 anthropogenic and biogenic fine (ABF) species infrastructure that incorporates secondarily
216 produced species such as sulfate and organics (both of which are dominated by fine mode
217 particles [< 1 μm]). Aerosol properties for each specie are defined in bulk and specific size
218 distributions are not considered.

219 NAAPS-RA optical properties are defined using species-dependent mass scattering,
220 absorption, and extinction efficiencies (α_{ext}, α_{scat}, and α_{abs}, respectively; Table 2) and the Hänel
221 (1976) formulation of the light scattering hygroscopic growth function *f*:
222

$$b_{scat,i}(\lambda, x, y, z) = c_i(x, y, z)\alpha_{scat,i}(\lambda) f_i[RH(x, y, z)] \quad (1)$$

$$f_i[RH(x, y, z)] = \left[\frac{100 - RH}{100 - RH_o}\right]^{-\gamma_i} \quad (2)$$

$$b_{abs,i}(\lambda, x, y, z) = c_i(x, y, z)\alpha_{abs,i}(\lambda) \quad (3)$$

$$b_{ext,i}(\lambda, x, y, z) = b_{scat,i}(\lambda, x, y, z) + b_{abs,i}(\lambda, x, y, z) \quad (4)$$

$$\tau_i(\lambda, x, y) = \int b_{ext,i}(\lambda, x, y, z)\, dz \quad (5)$$

$$\tau(\lambda, x, y) = \sum_{i=1}^{4} \tau_i(\lambda, x, y) \quad (6)$$

223
224 Here, $b_{scat,i}$, $b_{abs,i}$, and $b_{ext,i}$ are the scattering, absorption, and extinction coefficients,
225 respectively, at a given wavelength (λ; λ = 550 nm for this study), and c_i is the mass
226 concentration of species *i*. The horizontal coordinates (x, y) represent the longitudinal and

https://doi.org/10.5194/acp-2021-870
Preprint. Discussion started: 30 November 2021


Atmospheric Chemistry and Physics Discussions

latitudinal dimensionality (m), respectively, of each 1° grid box, while z (m) is the midpoint altitude of a given pressure layer. Each pressure layer has a unique thickness dz that increases with altitude. For f(RH), RH is the humidified relative humidity, RH_o is a dry reference relative humidity (30%), and γ_i is an empirical species-dependent hygroscopic growth parameter.

Vertical integrals then provide the speciated optical depths τ_i, which are then added to obtain total optical depth τ. Quality-controlled and assured Moderate Resolution Imaging Spectroradiometer (MODIS) and Multi-angle Imaging SpectroRadiometer (MISR) AOT data (Zhang and Reid, 2006; Hyer et al., 2011; Shi et al., 2011) are assimilated through the Navy Atmospheric Variational Data Assimilation System (NAVDAS) for AOT (NAVDAS-AOT; Zhang et al., 2008) into the model to create a final reanalysis product. When MODIS AOT data are assimilated into NAAPS, τ_i is adjusted proportionally for each species. Corrections in τ_i are converted to changes in c_i using the optical properties for that species and the simulated meteorological conditions (e.g., RH).

As discussed above, frequent cloud cover over SEA often interferes with satellite retrievals of AOT for the region. Thus, it is unsurprising that only 0 – 10 quality-controlled and assured MODIS retrievals were assimilated into NAAPS-RA per 1° grid for the region over the 6-week period relevant to the campaign (Fig. S1a). This was far fewer assimilations compared to other locations of the world, yet fairly consistent with other regions located along the intertropical convergence zone (ITCZ; Fig. S1b).

For this study, NAAPS-RA data were extracted at specific locations along each flight track with nearest neighbor interpolation spatially and temporally. For this study, lower bounds of the integrals in Equation 5 corresponded to the lower range of the HSRL-2 (~145 m) while upper bounds either corresponded to the highest altitude available in the HSRL-2 data or the MLH (~500 – 700 m; Sect. 3.1). This is discussed in greater detail below.

https://doi.org/10.5194/acp-2021-870
Preprint. Discussion started: 30 November 2021

Atmospheric Chemistry and Physics Discussions

Table 2. Optical properties for the four aerosol types considered in NAAPS-RA at 550 nm. "ABF" stands for anthropogenic and biogenic fine and "SSA" stands for single scattering albedo.

	α_{ext} (m^2 g^{-1})	α_{scat} (m^2 g^{-1})	α_{abs} (m^2 g^{-1})	γ	SSA
ABF	3.48	3.13	0.35	0.5	0.90
Dust	0.59	0.52	0.07	0	0.88
Smoke	4.49	3.99	0.50	0.18	0.89
Sea salt	1.42	1.41	0.01	0.46	0.99

https://doi.org/10.5194/acp-2021-870
Preprint. Discussion started: 30 November 2021


Atmospheric Chemistry and Physics Discussions

2.4 Strategy to Evaluate NAAPS-RA Performance

NAAPS-RA model performance was evaluated in light extinction phase space in two parts: (1) assessing how well the model simulated remotely sensed observable AOT and aerosol extinction coefficients for the entire campaign, and (2) concentrating on four case studies to attribute errors in simulated AOTs and extinction coefficients to errors in modeled RH, particle hygroscopic growth, and dry extinction. Details for how each part was completed are provided in the following sections.

2.5 Mixed Layer Heights

MLHs were derived from dropsonde vertical profiles of water vapor mixing ratio (henceforth referred to as "mixing ratio"), potential temperature (θ), temperature, and dew point temperature. The MLH was visually and somewhat subjectively determined by three methods: (i) the altitude at which temperature and dew point temperature "pinched" together, (ii) where the maximum vertical gradient in θ began (Seidel et al., 2010), and (iii) where the mixing ratio abruptly decreased after having been relatively uniform within the first few hundred meters above the surface (Betts and Albrecht, 1987) (see Fig. 1.5 in Stull, 1988 for a simultaneous depiction of these three methods). Rigorously, the altitude at which temperature and dew point temperature "pinched" together marked either cloud base or the base of a temperature inversion, both of which are commonly used to classify the MLH (Reid et al., 2017; Seidel et al., 2010; Seibert, 2000). The HSRL-2 MLH product (Scarino et al., 2014) quantifies the MLH by considering gradients in aerosol backscatter profiles and was used to quantify the MLH between dropsonde release points. The overall MLH for a given flight was defined as the average of all MLHs available via dropsonde and HSRL-2 data.

2.6 Selection of NAAPS-RA and HSRL-2 Data

NAAPS-RA data were extracted along each flight track at locations spatially and temporally coincident with the release of dropsondes to take advantage of the atmospheric vertical profile data. Specifically, NAAPS-RA data were selected for the 1° grid box containing the release point of each dropsonde and for the 6-hour period overlapping with the time of release. If multiple dropsondes were released in the same 1° grid and within the same 6-hour period, the data from each dropsonde were each individually compared to the same NAAPS-RA data for that grid. Dropsondes were only released when the P-3 was over the ocean. However, at a 1º resolution, coastal comparisons can be problematic. When a land mass protruded into the 1° grid box relevant to a dropsonde release point, these "land-contaminated" data were replaced with the NAAPS-RA nearest neighboring grid that encompassed only open water at the surface. We acknowledge that comparing airborne observations in one location to model simulations for an adjacent grid introduced some systematic error into our analysis, especially in the presence of steep gradients in aerosol properties and meteorological conditions. This systematic error affected some flights more than others. For example, all original NAAPS-RA grids had to be replaced for RF18, which sampled pollution in and around Manila, while no replacements were necessary for RFs 2, 11, 12, 13, and 19 (Fig. S2).

HSRL-2 data were filtered to isolate those with columnar retrievals of aerosol extinction that extended below 300 m. These data were filtered again to isolate retrievals of aerosol extinction (355, 532, 1064 nm) and 355-532 nm Angstrom exponent that were as temporally and spatially coincident as possible with dropsonde releases, which also ensured the HSRL-2 data were spatially and temporally coincident with NAAPS-RA data. If HSRL-2 data were

https://doi.org/10.5194/acp-2021-870
Preprint. Discussion started: 30 November 2021


Atmospheric Chemistry and Physics Discussions

unavailable within 50 minutes of a dropsonde release, the corresponding NAAPS-RA data were removed from the AOT and extinction analyses.

2.7 AOT

HSRL-2 532 nm aerosol extinction coefficients were converted to 550 nm using either the 355-532 nm Angstrom exponent provided or an Angstrom exponent calculated from extinction coefficients at 532 and 1064 nm if 355-532 nm Angstrom exponent data were unavailable. These retrievals typically began at ~145 m above the surface (to avoid surface return) and continued at a 15-m grid spacing (150-m resolution) to just below the aircraft's altitude. The derived HSRL-2 550 nm extinction coefficients were integrated across two altitude ranges: (i) ~145 m to just below the aircraft's altitude, and (ii) ~145 m to the mean MLH for each flight. These integrals served as the "ground truth" for total AOT and AOT in the mixed layer (AOT_{ML}), respectively, to which we compared the corresponding NAAPS-RA AOT and AOT_{ML} simulations. Under typical conditions, the total systematic error for HSRL-2 532 nm extinction coefficients is estimated to be less than 0.01 km^{-1}. Airborne HSRL measurements have been used to assess regional model representations of aerosol backscatter and extinction profiles from the Weather Research and Forecasting model coupled with Chemistry (WRF-Chem; Fast et al., 2011, 2012), as well as AOT derived from passive remote sensors (Shinozuka et al., 2013; Knobelspiesse et al., 2011; Kassianov et al., 2010).

To achieve as robust a comparison as possible, corresponding NAAPS-RA AOT and AOT_{ML} values were calculated by adding fine and coarse 550 nm aerosol extinction coefficients reported for each pressure layer and integrating the total extinction coefficients over the same two altitude ranges as in the corresponding HSRL-2 dataset. Corresponding NAAPS-RA and HSRL-2 AOT and AOT_{ML} values were then compared to identify certain flights and/or environmental conditions that prompted better or worse agreement.

Mean MLHs were ~500 – 700 m (Sect. 3.1), which greatly limited the number of extinction coefficients available for calculating AOT_{ML}. Specifically, only 3 – 4 (2 – 3) HSRL-2 (NAAPS-RA) independent extinction coefficients were reported in the ML per vertical extinction profile. However, since HSRL-2 extinction coefficients were interpolated to 15-m grid spacing, 22 – 36 HSRL-2 extinction coefficients were actually used to calculate the "ground truth" AOT_{ML}.

2.8 Vertically Resolved Extinction Coefficient

To explore NAAPS-RA performance as a function of altitude, we compared extinction coefficients within three altitude layers: (i) 145 – 500 m, (ii) 500 – 1500 m, and (iii) above 1500 m. NAAPS-RA data provided one fine and one coarse extinction coefficient at the midpoint of each pressure layer, the sum of which gave a total extinction coefficient to represent that pressure layer. We extracted HSRL-2 550 nm extinction coefficients retrieved at altitudes closest to the midpoint altitude of each model pressure layer in order to match retrievals in model space. For example, although ~350 HSRL-2 extinction coefficients were available per column, the ~11 coefficients most vertically aligned with NAAPS-RA pressure layer midpoints were selected and compared to the corresponding NAAPS-RA extinction coefficients. Comparisons were made at very similar altitudes (R^2 = 1.00, bias = 5.00 m, root mean square error [RMSE] = 48.19 m; Fig. S3a), with 2, 3, and 2 – 6 comparisons typically made for altitude layers of 145 – 500 m, 500 – 1500 m, and >1500 m, respectively (e.g., Fig. S3b).

Dropsonde data were also extracted at the altitudes closest to the midpoint altitude of each model pressure layer (Fig. S3c). We substituted the isolated dropsonde RH values for

https://doi.org/10.5194/acp-2021-870
Preprint. Discussion started: 30 November 2021

Atmospheric Chemistry and Physics Discussions

NAAPS-RA RH values and recalculated the extinction coefficients, total AOT, and AOT_{ML}, which were again compared to those retrieved with the HSRL-2. Improvements and/or changes in agreement provided insight on (i) the relationship between model error in RH and model error in extinction, and (ii) how sensitive NAAPS-RA extinction outputs were to changes in RH.

2.9 In Situ Mass Concentrations

Equations 1 and 3 show dry particle mass concentrations are an important component in simulating particle light extinction. Fine and coarse in situ mass concentrations were calculated to evaluate the accuracy of those simulated by NAAPS-RA in the ML. In situ fine mass was characterized as the sum of AMS mass concentrations for organic aerosol (OA), sulfate (SO_4^{2-}), nitrate (NO_3^-), ammonium (NH_4^+), and chloride (Cl^-). Previous studies have examined the ability of the AMS to capture total fine particle mass by comparing to fine mass concentrations derived with other instruments, such as particle-into-liquid samplers (PILSs; e.g., Takegawa et al., 2005), optical particle counters (OPCs; e.g., Middlebrook et al., 2012 and references therein), and tapered element oscillating microbalances (TEOMs; e.g., Salcedo et al., 2006). AMS collection efficiency (CE) is adjusted to reach mass closure with the aforementioned and related instruments, with a CE of 0.5 being most common (Middlebrook et al., 2012 and references therein). AMS CE was set to 1 for the campaign based on comparison with coincident PILS measurements. This, in conjunction with the instrument's insensitivity to submicron dust and sea salt, indicates AMS mass concentrations represented a lower limit of true dry fine mass.

Coarse particle mass concentrations were calculated using FCDP size distributions and assuming all coarse particles were sea salt. In support of this, Hilario et al. (2020a) found crustal-marine particles to contribute 57% of the coarse particle mass (1.15 – 10 μm) in the South China Sea in late September. As the FCDP sampled particles under ambient conditions, the dry particle diameter (D_p) range was calculated for each bin using the procedure described on pages 54 – 55 in Lewis and Schwartz (2004). Specifically, equations modeling the deliquescence growth curve for sea salt were used to determine relationships between the radii of sea salt particles at ambient RH (r), at 80% RH (r_{80}), and in dry conditions (r_{dry}):

$$\frac{r}{r_{80}} = \frac{0.54}{(1-RH)^{\frac{1}{3}}} \; for\; RH > 93\% \tag{7}$$

$$\frac{r}{r_{80}} = \frac{0.67}{(1-RH)^{\frac{1}{4}}} \; for\; RH < 93\% \tag{8}$$

$$r_{dry} = \frac{r_{80}}{2} \tag{9}$$

For each FCDP size distribution, radii marking the edges of each size bin were set equal to r, while airborne meteorological data provided temporally-coincident ambient RH values. The dry size distributions were then integrated using the density of sea salt (2.20 g cm^{-3}; Seinfeld and Pandis, 2016) to arrive at total dry coarse particle mass concentration.

There are several uncertainties associated with quantifying coarse mass this way. First, this correction is very sensitive at RH > ~90% where sea salt exhibits large growth factors (e.g., Lewis and Schwartz, 2004). RHs above this threshold were common in the ML throughout the campaign (as will be shown in Sect. 3.3). The resulting large differences between ambient and

https://doi.org/10.5194/acp-2021-870
Preprint. Discussion started: 30 November 2021


Atmospheric Chemistry and Physics Discussions

dry particle radii corresponded to even larger corrections for dry particle volume, and therefore, dry particle mass. Additionally, there are known challenges in using OPCs (such as the FCDP) to accurately quantify coarse particle mass concentrations. The FCDP assumes the refractive index of water to derive sizes for all particles it samples, which can introduce error when particles are not liquid. However, it is inconclusive as to whether coarse mass concentrations derived from OPCs tend to be negatively or positively biased. For example, Reid et al. (2003, 2006) found coarse mode OPCs to overestimate the size of coarse particles (e.g., sea salt and dust), while other works have found OPCs to underestimate coarse mass concentrations (Kulkarni and Baron, 2011; Burkart et al., 2010). Despite these limitations, our derived coarse masses were still useful in roughly evaluating the corresponding NAAPS-RA simulations.

2.10 Case Studies

As mentioned above, the Philippines region is influenced by a range of aerosol types (Hilario et al., 2021). Aerosol models, such as NAAPS-RA, are heavily parameterized and are often challenged by the properties of individual air masses. To provide context to the bulk comparisons, four case studies were examined to assess model sensitivity and performance across a diverse range of aerosol conditions. Here we focus on model performance in the ML, which is representative of CCN concentrations entering cloud base and visibility and air quality at the surface. Evaluation of NAAPS-RA performance in the entrainment zone and planetary boundary layer/lower free troposphere regions is a subject of a subsequent study. NAAPS-RA data were selected for the 1° grid where the P-3 spent the most time in the ML. Only one vertical profile of dropsonde RH and one vertical profile of HSRL-2 extinction was used for each case study. Due to limited data availability, in situ γ values and fine and coarse particle mass concentrations obtained outside of this 1° grid were used in the analysis. We verified these parameters were relatively uniform in and around the 1° grid before making this decision.

2.10.1 Case Study Descriptions

Each case study is introduced below, along with a brief explanation for why it was chosen. Note that the monsoonal transition occurred from 23 – 24 September 2019.

- *Clean (RF19: 5 October 2019):* The location (Fig. 1) and relatively low observed and simulated aerosol particle loadings (Fig. S4a) indicated the P-3 sampled a relatively clean marine environment as compared to the rest of the campaign.
- *Biomass Burning Smoke (RF9: 15 September 2019):* Flight notes and photographs from RF9 revealed exceptionally hazy/smoky conditions. The location and timing of this flight were conducive to sampling smoke transported from the MC (Fig. S4b).
- *Asian pollution (RF17: 1 October 2019):* The aircraft sampled relatively high concentrations of SO_4^{2-} (~8 µg m^{-3}; measured with the AMS) in the ML during this flight. The location of the flight tracks and simulated wind patterns at 925 hPa made it reasonable to assume the enhanced SO_4^{2-} was from East Asian outflow (Fig. S4c; e.g., Lim et al., 2018; Hilario et al., 2021).
- *Mixed (RF10: 16 September 2019):* We examined γ and f(RH) along each flight track to identify cases in which air masses with noticeably different hygroscopicities converged within a 1° grid box in the ML. For the case chosen, relatively hygroscopic aerosol (East Asian outflow) dominated the northwestern part of the box (Fig. S5; γ = ~0.3; f(RH) = ~1.6), while more hydrophobic aerosol (aged smoke from the MC) dominated the rest of

https://doi.org/10.5194/acp-2021-870
Preprint. Discussion started: 30 November 2021


Atmospheric Chemistry and Physics Discussions

the box (γ = ~0.0; *f*(RH) = ~1.0). NAAPS-RA also simulated the convergence of these two air masses near the location of this grid (Fig. S4d).

https://doi.org/10.5194/acp-2021-870
Preprint. Discussion started: 30 November 2021

Atmospheric Chemistry and Physics Discussions

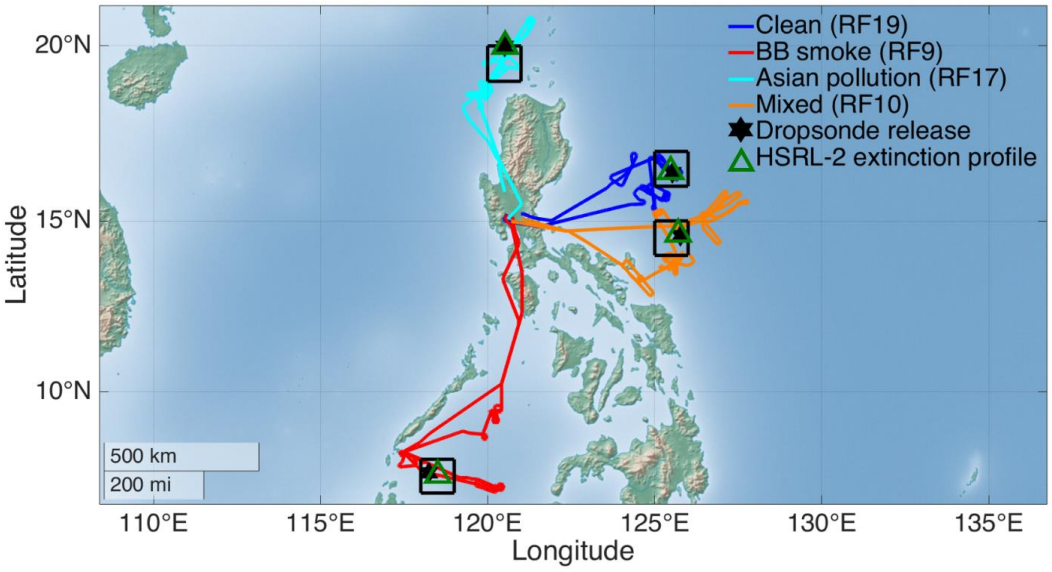

Figure 1. Flight tracks and specific locations relevant to the case studies. Open green triangles denote where vertically resolved HSRL-2 data were extracted, black six-pointed stars indicate dropsonde release points, and black squares outline the 1° grids relevant to the NAAPS-RA datasets. "BB" stands for biomass burning.

https://doi.org/10.5194/acp-2021-870
Preprint. Discussion started: 30 November 2021

Atmospheric Chemistry and Physics Discussions

437 **2.10.2 Extinction Coefficient Evaluation**

438 For each case study, NAAPS-RA extinction coefficients were initially compared to those
439 retrieved with the HSRL-2 within the ML. Dropsonde RH values were then substituted into the
440 model to observe how extinction coefficients changed when only RH was varied. Then observed
441 γ values were used in Equation 2 to assess NAAPS-RA extinction performance when only this
442 parameter was corrected. Finally, observed γ and dropsonde RH values were both used in the
443 model to evaluate performance when the entire *f*(RH) term was corrected. To account for the
444 range of in situ γ values observed during a given case study, the mean γ as well as γ values one
445 standard deviation above and below the mean were used in Equation 2, resulting in a range of
446 extinction coefficient outputs.

447 After correcting the *f*(RH) term, any remaining discrepancies between modeled and
448 retrieved extinction coefficients were attributed to model errors in dry extinction ($b_{ext,dry}$). We
449 determined the required dry extinction ($b_{ext,dry,req}$) to reach extinction agreement with the
450 HSRL-2 using the following relationship:
451

$$b_{ext,HSRL-2} = \left(b_{ext,dry,req}\right)\left(f[RH]\right)_{corrected,} \quad (10)$$

452
453 which is derived from Equations 1, 3, and 4 (note that $\alpha_{ext} = \alpha_{scat} + \alpha_{abs}$) and assumes that
454 particle absorption is affected by hygroscopic growth. In situ single scattering albedo (SSA)
455 values were above 0.96 for all case studies (except "clean," in which ML SSA data were
456 unavailable), indicating that total particle extinction was dominated by scattering. Thus,
457 assuming a dependence of particle absorption on hygroscopic growth was unlikely to alter our
458 results significantly.
459
460 **3. Results and Discussion**
461 **3.1 Mixed Layer Heights**

462 Mean MLHs across the campaign were relatively uniform (Table S2), ranging from ~500
463 – 700 m. Mean values were largely dictated by the HSRL-2 MLH product as there were 1 – 3
464 orders of magnitude more MLH retrievals than there were dropsonde releases. Mean MLHs
465 estimated from the three methods relying on dropsonde data were all negatively (positively) biased
466 for 13 (3) of the 19 RFs in reference to the overall mean. Interestingly, dropsonde MLHs were
467 positively biased for three of the first four RFs, and were almost always negatively biased for the
468 remaining 15 RFs. Dropsonde MLHs (means of 353± 223, 308 ± 147, 344 ± 215 m for the methods
469 using dew point temperature and temperature, θ, and mixing ratio, respectively) were especially
470 lower than HSRL-2 retrievals (572± 198 m) for RF 18, which sampled pollution in and around
471 Manila. This may have been the result of pollution detrainment out of the mixed layer and into the
472 free troposphere above it.

473 It is worth noting dropsondes were occasionally released in locations with unique
474 meteorological conditions (e.g., cold pools, convective systems, outflow boundaries) that were not
475 always reflective of the typical meteorological conditions observed throughout a given flight.
476 Nonetheless, both the mean MLHs, as well as those determined by the four methods described in
477 Sect. 2.5, were consistent with MLH observations over the northern Philippine Sea (Zhu et al.,
478 2018) in the boreal fall.
479

https://doi.org/10.5194/acp-2021-870
Preprint. Discussion started: 30 November 2021

Atmospheric Chemistry and Physics Discussions

3.2 AOT and Extinction Comparison using NAAPS-RA RHs

Over the course of 19 RFs, the P-3 sampled a wide variety of aerosol and meteorological conditions. Air masses and aerosol features encountered included both clean and smoky conditions over the Sulu Sea (RFs 4 and 9, respectively), relatively clean conditions as well as aged smoke over the Western Pacific (RFs 19 and 10, respectively), East Asian outflow (RFs 11, 13, 14, and 17), pollution in and around Manila (RF18), shipping emissions (e.g., RF16), emissions from a coal-fired power plant (RF8), and brief samplings over the Mayon Volcano (RF10). The aircraft also encountered land breezes, cold pools, convective cells, confluence and convergence lines, convective outflow bands from a tropical cyclone, as well as fair weather. NAAPS-RA data and HSRL-2 retrievals were compared at 2 – 17 locations per flight, with a total of 177 comparisons for the entire campaign. Multiple dropsondes were released within the same grid for several RFs, providing an opportunity to evaluate the model against a variety of atmospheric conditions occurring within a single grid over a period of several hours.

Overall, NAAPS-RA displayed good correlation with HSRL-2 retrievals for AOT (R^2 = 0.68, bias = 0.01, RMSE = 0.14; Fig. 2a) and AOT_{ML} (R^2 = 0.83; bias = 0.00; RMSE = 0.03; Fig. S6a). NAAPS-RA AOT simulations were especially good for RFs 2 and 19 (R^2 = 0.76, 0.89; bias = -0.03, -0.01; RMSE = 0.04, 0.02, respectively; Table S3), which experienced relatively clean conditions as well as periods of convection and rainfall. AOT_{ML} agreement was also good for RF2 (R^2 = 0.57; bias = -0.01; RMSE = 0.01; Table S4), as well as for RF9 (R^2 = 0.74; bias = -0.03; RMSE = 0.05), which sampled smoke from the MC advecting into the Sulu Sea.

NAAPS-RA struggled most in environments with steep gradients in meteorological conditions and aerosol properties. RF18, which sampled pollution in and around Manila, had the second largest negative bias for AOT (-0.10). This was likely because all NAAPS-RA grids had been replaced with neighboring grids that were farther from land. Steep gradients in simulated fine AOT between these locations (Figs. S7a-b) implied that the replaced NAAPS-RA grids contained drastically different atmospheric conditions compared to the original grids. Similarly, the greatest positive bias (0.26) was seen for RF10, which encountered convective systems, heavy rainfall, cold pools, and multiple outflow boundaries, while also sampling aged smoke particles from the MC and East Asian outflow. Seventeen dropsondes were released over an area covered by seven NAAPS-RA 1° grids during RF10. Therefore, model data for a single grid were compared to multiple observations and retrievals of various atmospheric conditions within that grid. NAAPS-RA assumed relatively polluted and smoky conditions for each grid, which would have generated positive biases whenever the aircraft sampled a relatively clean region within a given grid (e.g., flight notes mention the aircraft encountered “heavy rain” near a dropsonde release point, which means that part of the grid may have been relatively cleaner due to particle losses via wet scavenging).

Extinction coefficient analyses provided insight into the model’s strengths and weaknesses in the vertical dimension. NAAPS-RA showed the strongest correlation with HSRL-2 retrievals for extinction from 145 – 500 m (R^2 = 0.75; bias = 0.01 km^{-1}; RMSE = 0.08 km^{-1}; Fig. 2b), with decreasing correlation as altitude increased above this (R^2 = 0.69 and 0.26; bias = 0.00 and 0.00 km^{-1}; RMSE = 0.09 and 0.00 km^{-1} for 500 – 1500 m and > 1500 m, respectively; Fig. 2c-d). This is in agreement with the finding that NAAPS-RA showed stronger correlation for AOT_{ML} than for total AOT. Decreasing model accuracy with altitude could be occurring for a number of reasons. First, NAAPS-RA may be misrepresenting boundary layer height as there is typically a steep decrease in aerosol extinction between the boundary layer (BL) and free troposphere. The model could also be struggling to capture how aerosol particles mix between the BL and free troposphere.

https://doi.org/10.5194/acp-2021-870
Preprint. Discussion started: 30 November 2021


Atmospheric Chemistry and Physics Discussions

Finally, above 1500 m, model pressure layers are *at least* 500 m thick with only one extinction coefficient to represent an entire layer. In contrast, HSRL-2 data maintain 15-m grid spacing throughout a column. This increasing discrepancy in vertical resolution with altitude naturally reduced agreement.

AOT agreement was occasionally driven by error cancellations in extinction across the three altitude layers (Fig. 3). For example, modeled extinction coefficients were positively biased (0.02 km^{-1}; Table S5) from 145 – 500 m, negatively biased from 500 – 1500 m (-0.16 km^{-1}; Table S6), and unbiased above 1500 m (0.00 km^{-1}; Table S7) for RF9. Cancellations between these biases resulted in a small negative bias for AOT (-0.02). Similarly, RF17 had the second highest positive bias for extinction from 145 – 500 m (0.09 km^{-1}), but negative biases at higher altitudes resulted in a negative bias for AOT (-0.03).

Finally, the model failed to capture extinction variability from 145 – 500 m for several flights, such as RFs 8, 18, and 19, which sampled (i) outflow boundaries, diurnal changes in radiation, and plumes of pollution near Manila, (ii) pollution in and around Manila, and (iii) relatively clean conditions, respectively. For example, HSRL-2 extinction coefficients spanned two orders of magnitude (~0.001–0.05 km^{-1}) during RF19, while all NAAPS-RA simulations were nearly identical (~0.02 km^{-1}), despite being extracted for four different 1° grid boxes.

https://doi.org/10.5194/acp-2021-870
Preprint. Discussion started: 30 November 2021

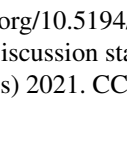

Atmospheric Chemistry and Physics Discussions

543

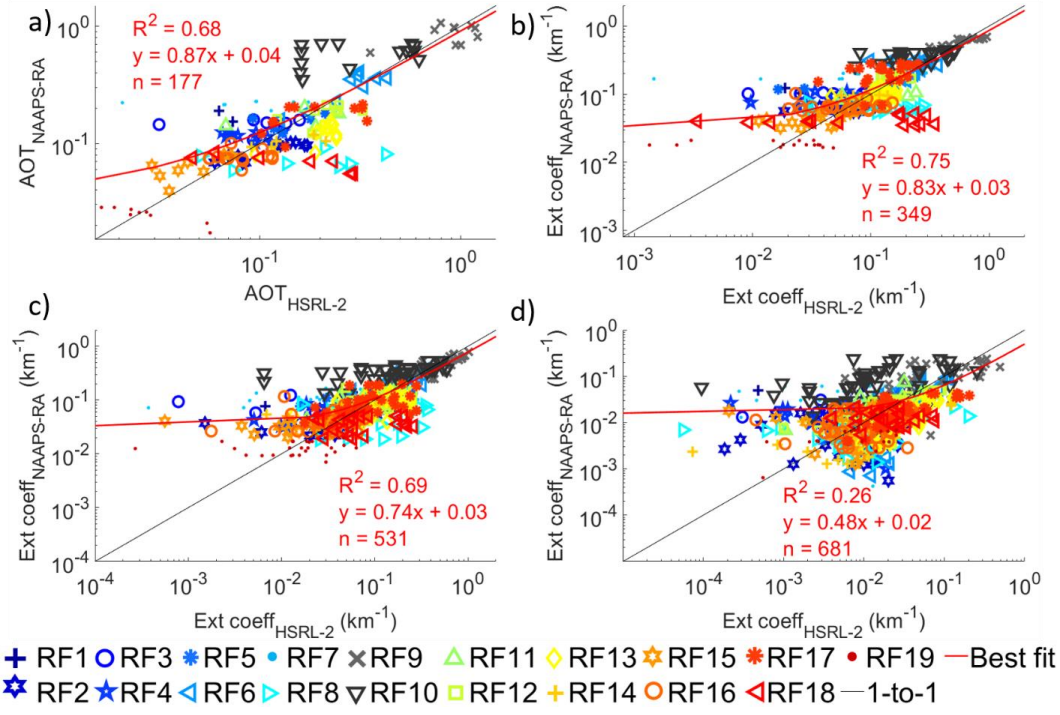

544
545

546 **Figure 2.** Comparison between simulated (NAAPS-RA) and retrieved (HSRL-2) (**a)** 550 nm
547 aerosol optical thickness (AOT), as well as 550 nm extinction coefficients **(b)** between 145 and
548 500 m, **(c)** between 500 and 1500 m, and (**d)** above 1500 m at various locations in each research
549 flight (RF). NAAPS-RA extinction coefficients were calculated using relative humidity (RH) from
550 NAAPS-RA.

https://doi.org/10.5194/acp-2021-870
Preprint. Discussion started: 30 November 2021

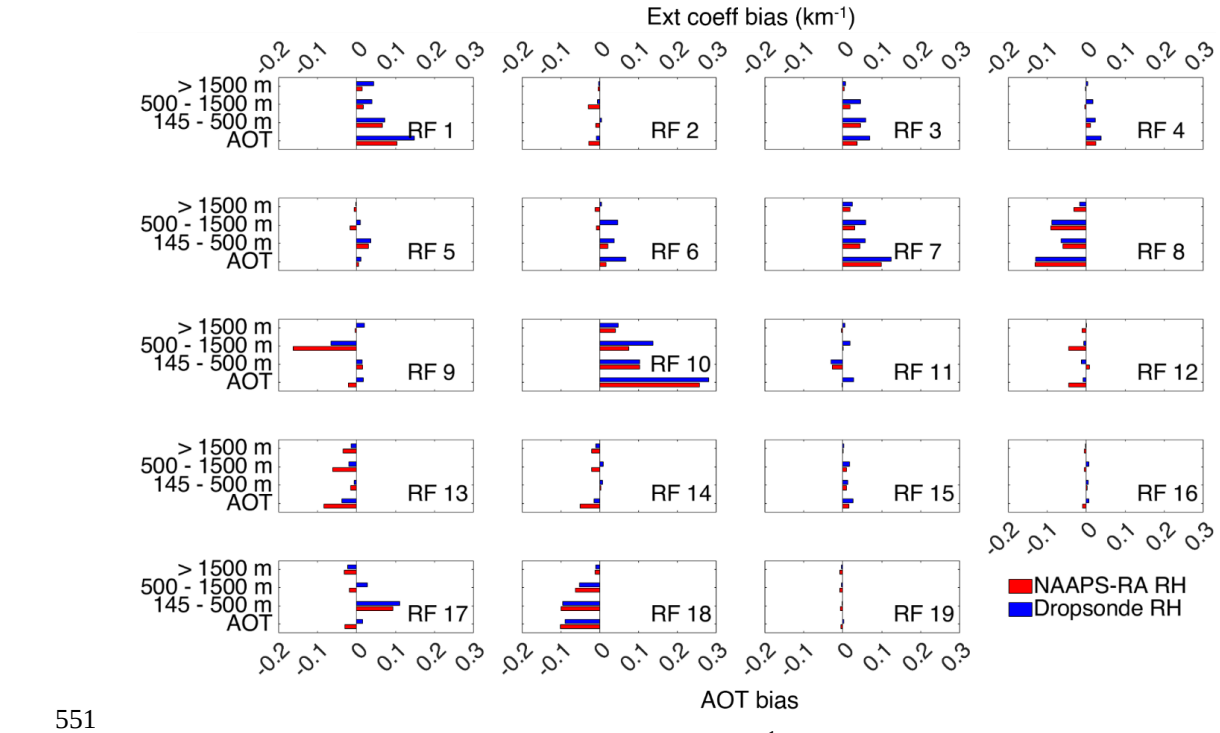

Figure 3. Biases in AOT and extinction coefficients (km^{-1}) calculated with NAAPS-RA RHs (red bars) and dropsonde RHs (blue bars) for each RF. Biases in extinction are reported for three altitude layers, which are denoted with the labels "145 – 500 m," "500 – 1500 m," and "> 1500 m."

https://doi.org/10.5194/acp-2021-870
Preprint. Discussion started: 30 November 2021


Atmospheric Chemistry and Physics Discussions

3.3 AOT and Extinction Comparison Using Dropsonde RHs

We expected NAAPS-RA extinction to be responsive to changes in RH due to the humid environment and exponential increase in *f*(RH) at high RH (Equation 2). For example, Beyersdorf et al. (2016) found variability in RH to cause up to 62% of the spatial variability and 95% of the diurnal variability in ambient extinction on days with RH > 60% at a location on the United States East Coast.

In this study, NAAPS-RA RHs were negatively biased and showed poor agreement with dropsonde RHs in each altitude layer (R^2 = 0.15, 0.17, and 0.43; bias = -4.9, -7.7, and -2.3% ; RMSE = 8.1, 14.4, 18.1% for altitudes below 500 m, 500 – 1500 m, and > 1500 m, respectively; Fig. 4a-c). The lack of correlation for RH across the campaign (R^2 = 0.49; Fig. S8a) was a surprising result considering NAAPS-RA showed excellent agreement with the dropsondes for temperature (R^2 = 0.99; Fig. S8b) and specific humidity (R^2 = 0.92; Fig. S8c), and that comparisons were made at nearly identical altitudes (R^2 = 1.00; Fig. S8d). Further work is needed to fully understand the poor agreement for RH.

As expected, NAAPS-RA AOT and extinction coefficients increased when negatively biased NAAPS-RA RHs were replaced with dropsonde values. Specifically, biases in AOT and extinction either became more positive or less negative for all flights and altitude layers when dropsonde RHs were used, except for extinction coefficients for RF12 from 145 – 500 m (Table S8). However, agreement for AOT, AOT_{ML}, and extinction with the HSRL-2 did not improve across the campaign (Figs. 5a-d and S6b) as R^2 values did not change significantly at any altitude. Thus, model errors in AOT and extinction were likely due to errors in other parameters. The next section examines other sources of error by assessing NAAPS-RA simulations for RH, dry extinction, and particle hygroscopic growth in the ML for four case studies.

https://doi.org/10.5194/acp-2021-870
Preprint. Discussion started: 30 November 2021

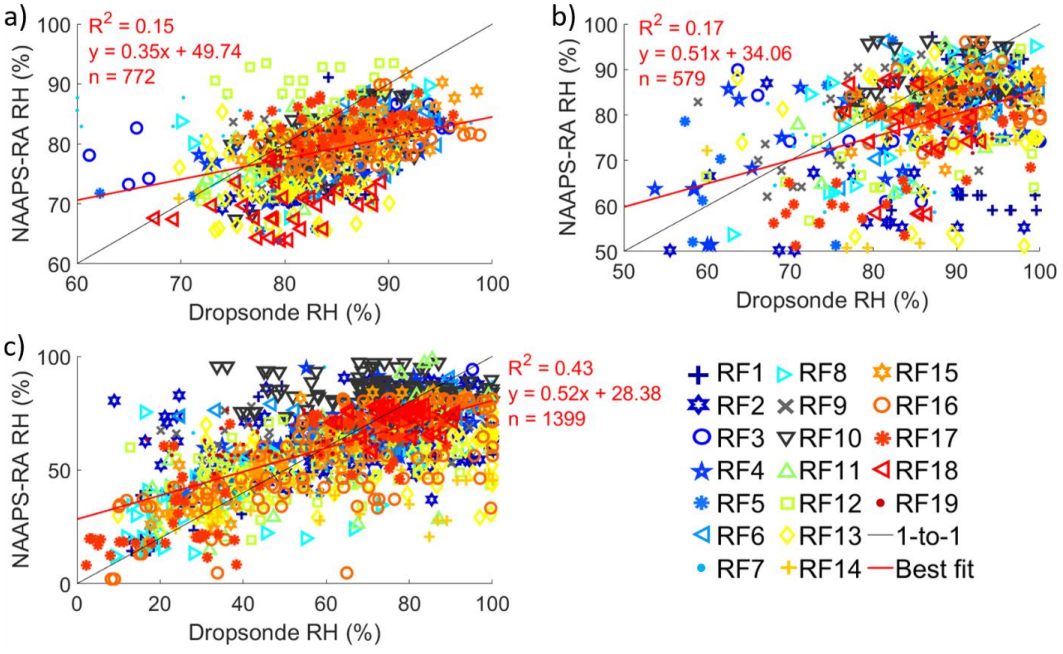

579

580 **Figure 4.** Comparison between simulated (NAAPS-RA) and measured (dropsonde) RH **(a)**
581 below 500 m, **(b)** between 500 and 1500 m, and (**c)** above 1500 m at various locations in each
582 RF.

https://doi.org/10.5194/acp-2021-870
Preprint. Discussion started: 30 November 2021

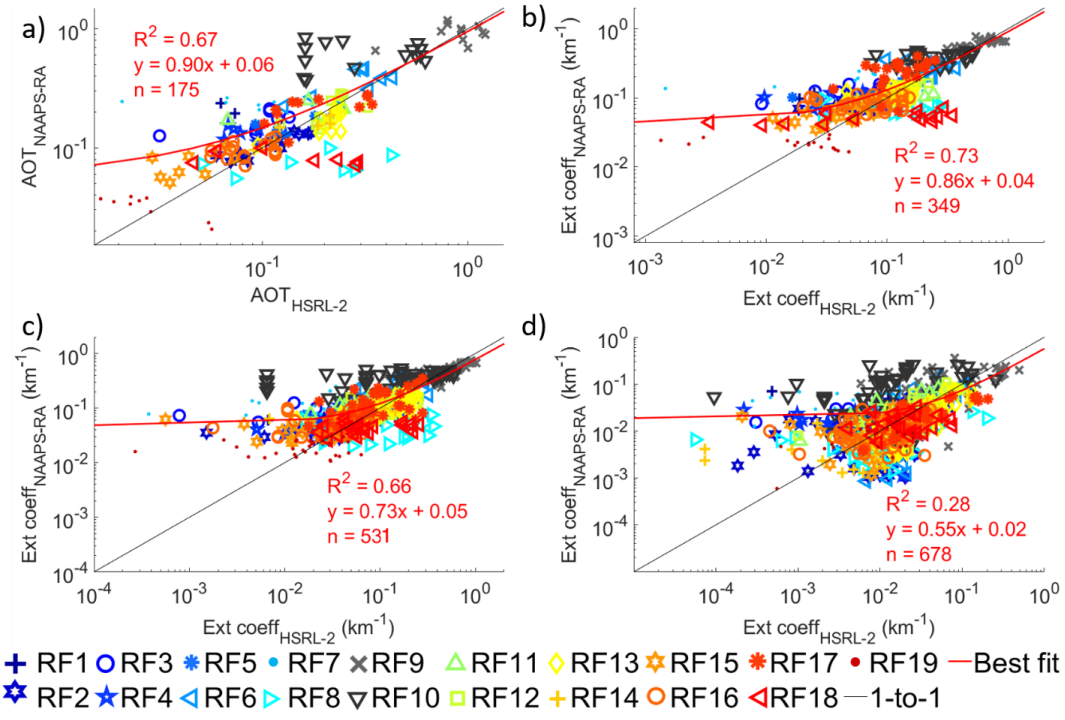

Figure 5. Comparison between simulated (NAAPS-RA) and retrieved (HSRL-2) (**a)** 550 nm aerosol optical thickness (AOT), as well as 550 nm extinction coefficients **(b)** between 145 and 500 m, **(c)** between 500 and 1500 m, and (**d)** above 1500 m at various locations in each RF. NAAPS-RA extinction coefficients were calculated using dropsonde RH data.

https://doi.org/10.5194/acp-2021-870
Preprint. Discussion started: 30 November 2021


Atmospheric Chemistry and Physics Discussions

589 **3.4 Case Studies**
590 **3.4.1 Clean (RF19)**
591 RF19 sampled the cleanest conditions for the entire campaign and provided an opportunity
592 to evaluate NAAPS-RA when AOT was very low (HSRL-2 AOT and AOT_{ML} ranged from 0.02 –
593 0.06 and 0.01 – 0.02, respectively). This period was associated with a mild tropical disturbance
594 and advection of clean marine air from southeast of the Philippines.
595 For this single comparison, NAAPS-RA showed a negative bias for mixed-layer extinction,
596 AOT_{ML}, and AOT (MLH = 578 m; b_{ext} bias = -0.03 km^{-1}; HSRL-2 b_{ext} mean = 0.04 ± 0.00 km^{-1};
597 AOT_{ML} bias = -0.01; AOT bias = -0.04; Table 3) and failed to capture the vertical profile of
598 extinction correctly (Fig. 6a). Total modeled extinction was dominated by coarse (i.e., sea salt and
599 dust) particles in the ML, whereas fine (i.e., smoke and ABF) and coarse particles contributed
600 evenly to extinction above the MLH when both NAAPS-RA RHs and dropsonde RHs were used
601 (Figs. S9a and S9b, respectively). Both the bias and shape of the NAAPS-RA extinction profile
602 were largely unchanged when NAAPS-RA RHs were replaced with those from the dropsonde (Fig.
603 6b), which is unsurprising for two reasons: (i) vertically-resolved model and dropsonde RHs were
604 similar in the ML (Fig. 6c), and (ii) variability in extinction did not appear to be highly sensitive
605 to particle hygroscopic growth. Specifically, NAAPS-RA and HSRL-2 extinction profiles did not
606 follow the vertical profile of RH, and the highest extinction values were observed when RHs were
607 lowest. A mean in situ γ value of 0.20 ± 0.16 indicated particles were less hygroscopic than has
608 been observed for other clean marine environments ($0.38 \leq \gamma \leq 0.73$; Titos et al., 2016 and
609 references therein). NAAPS-RA expected dust to be a dominant aerosol type (Fig. S9c), but images
610 of HSRL-2 532 nm particle depolarization ratios show values below 0.05 in the ML, implying dust
611 was likely not a dominant particle type (Fig. S10; Groß et al., 2013; Burton et al., 2013). This type
612 of speciation confusion within the NAAPS model during pristine conditions is a byproduct of the
613 nature of transport models and data assimilation. When AOTs are low, differences between species
614 become noisy and data assimilation will work to uniformly modulate this noise. Here, however,
615 we are more interested in the overall extinction bias, and we save a full assessment of NAAPS-RA
616 speciation for a later paper.
617 NAAPS-RA slightly overestimated particle hygroscopic growth, and correcting γ induced
618 negligible changes in extinction (bias for b_{ext} remained at -0.03 km^{-1}). Thus, extinction
619 disagreement was driven mostly by underestimated dry extinction. NAAPS-RA simulations for
620 fine mass concentrations fell within the range of those derived from the AMS, but modeled coarse
621 mass concentrations were typically much higher than those derived from FCDP size distributions
622 (Fig. 6d). We acknowledge that there is much uncertainty involved with deriving coarse mass
623 concentrations (as described in Sect. 2.9), especially considering ambient RHs ranged from 76 –
624 100% in the ML during RF19. Nonetheless, NAAPS-RA dry extinction would need to increase in
625 order to achieve AOT and extinction agreement with the HSRL-2, and future works can investigate
626 whether this would require an increase in modeled particle mass concentrations, mass extinction
627 efficiency, or both.

https://doi.org/10.5194/acp-2021-870
Preprint. Discussion started: 30 November 2021

Atmospheric Chemistry and Physics Discussions

Table 3. Optical properties and summary statistics (means [standard deviations in parentheses], biases, and root mean square errors [RMSEs]) for NAAPS-RA/HSRL-2 comparisons for each case study. AOT_{ML} denotes AOT within the mixed layer (ML). Biases and RMSEs for b_{ext} ($b_{ext,dry}$) represent deviations between NAAPS-RA and HSRL-2 extinction coefficients (NAAPS-RA $b_{ext,dry}$ and $b_{ext,dry,req}$) at corresponding altitudes within the ML. Each case study is only a single comparison within a single 1° grid.

		Clean	Smoke	Asian pollution	Mixed
		RF19	RF9	RF17	RF10
HSRL-2	AOT	0.06	1.13	0.34	0.16
	AOT_{ML}	0.02	0.34	0.08	0.08
	Mean: b_{ext} (km^{-1})	0.04 (0.00)	0.72 (0.22)	0.18 (0.06)	0.17 (0.02)
NAAPS-RA Original	AOT	0.02	1.02	0.16	0.70
	AOT_{ML}	0.01	0.31	0.06	0.18
	Mean: b_{ext} (km^{-1})	0.02 (0.00)	0.63 (0.02)	0.17 (0.05)	0.41 (0.01)
	Bias: b_{ext} (km^{-1})	-0.03	-0.09	-0.02	0.24
	RMSE: b_{ext} (km^{-1})	0.03	0.23	0.10	0.24
	Mean: mass-weighted γ	0.27 (0.03)	0.21 (0.00)	0.42 (0.01)	0.25 (0.00)
	Mean: $b_{ext,dry}$ (km^{-1})	0.01 (0.00)	0.51 (0.03)	0.09 (0.01)	0.30 (0.01)
NAAPS-RA with Dropsonde RH	AOT_{ML}	0.01	0.36	0.10	0.20
	Mean: b_{ext} (km^{-1})	0.02 (0.00)	0.73 (0.05)	0.30 (0.09)	0.44 (0.03)
	Bias: b_{ext} (km^{-1})	-0.03	0.01	0.11	0.26
	RMSE: b_{ext} (km^{-1})	0.03	0.24	0.12	0.27
NAAPS-RA with In Situ γ[a]	AOT_{ML}	0.00/0.01 /0.01	0.16/0.16/0.16	0.04/0.05/0.05	0.12/0.14/ 0.16
	Mean: b_{ext} (km^{-1})	0.01 (0.00)/ 0.01 (0.00)/ 0.01 (0.01)	0.47 (0.03)/ 0.48 (0.03)/ 0.49 (0.03)	0.11 (0.02)/ 0.12 (0.02)/ 0.13 (0.03)	0.27 (0.01)/ 0.32 (0.01)/ 0.37 (0.01)
	Bias: b_{ext} (km^{-1})	-0.03/ -0.03/ -0.03	-0.25/ -0.24/ -0.23	-0.07/ -0.06/ -0.05	0.10/ 0.15/ 0.20
	RMSE: b_{ext} (km^{-1})	0.03/0.03/ 0.03	0.33/0.32/0.31	0.10/0.10/0.09	0.10/0.15/ 0.20
	Mean: in situ γ	0.20 (0.16)	-0.06 (0.02)	0.24 (0.06)	0.04 (0.12)
NAAPS-RA with Dropsonde RH and In Situ γ[a]	AOT_{ML}	0.00/0.01/ 0.01	0.15/0.15/0.16	0.05/0.06/0.08	0.12/0.14/ 0.17
	Mean: b_{ext} (km^{-1})	0.02 (0.00)/ 0.01 (0.00)/ 0.02 (0.00)	0.44 (0.02)/ 0.46 (0.02)/ 0.48 (0.02)	0.14 (0.01)/ 0.16 (0.02)/ 0.19 (0.03)	0.27 (0.01)/ 0.32 (0.01)/ 0.39 (0.01)
	Bias: b_{ext} (km^{-1})	-0.03/ -0.03/ -0.03	-0.27/ -0.26/ -0.24	-0.05/ -0.03/ 0.00	-0.10[b]/ 0.15/ 0.21
	RMSE: b_{ext} (km^{-1})	0.03/0.03/ 0.03	0.35/0.33/0.32	0.07/0.05/0.03	0.10/0.15/ 0.22
	Mean: $b_{ext,dry,req}$ (km^{-1})	0.04 (0.00)/ 0.03 (0.00)/ 0.03 (0.00)	0.84 (0.26)/ 0.80 (0.25)/ 0.77 (0.24)	0.12 (0.03)/ 0.10 (0.03)/ 0.09 (0.02)	0.20 (0.02)/ 0.16 (0.02)/ 0.13 (0.02)
	Bias: NAAPS-RA $b_{ext,dry}$(km^{-1})	-0.03/ -0.02/ -0.02	-0.33/ -0.30/ -0.26	-0.03/ -0.01/ 0.00	0.10/ 0.14/ 0.17
	RMSE: NAAPS $b_{ext,dry}$(km^{-1})	0.03/ 0.02/ 0.02	0.41/ 0.38/ 0.35	0.05/ 0.03/ 0.02	0.10/ 0.04/ 0.07

[a]The three values shown are based on calculations using the γ value one standard deviation below the mean, the mean, and one standard deviation above the mean, respectively.

https://doi.org/10.5194/acp-2021-870
Preprint. Discussion started: 30 November 2021

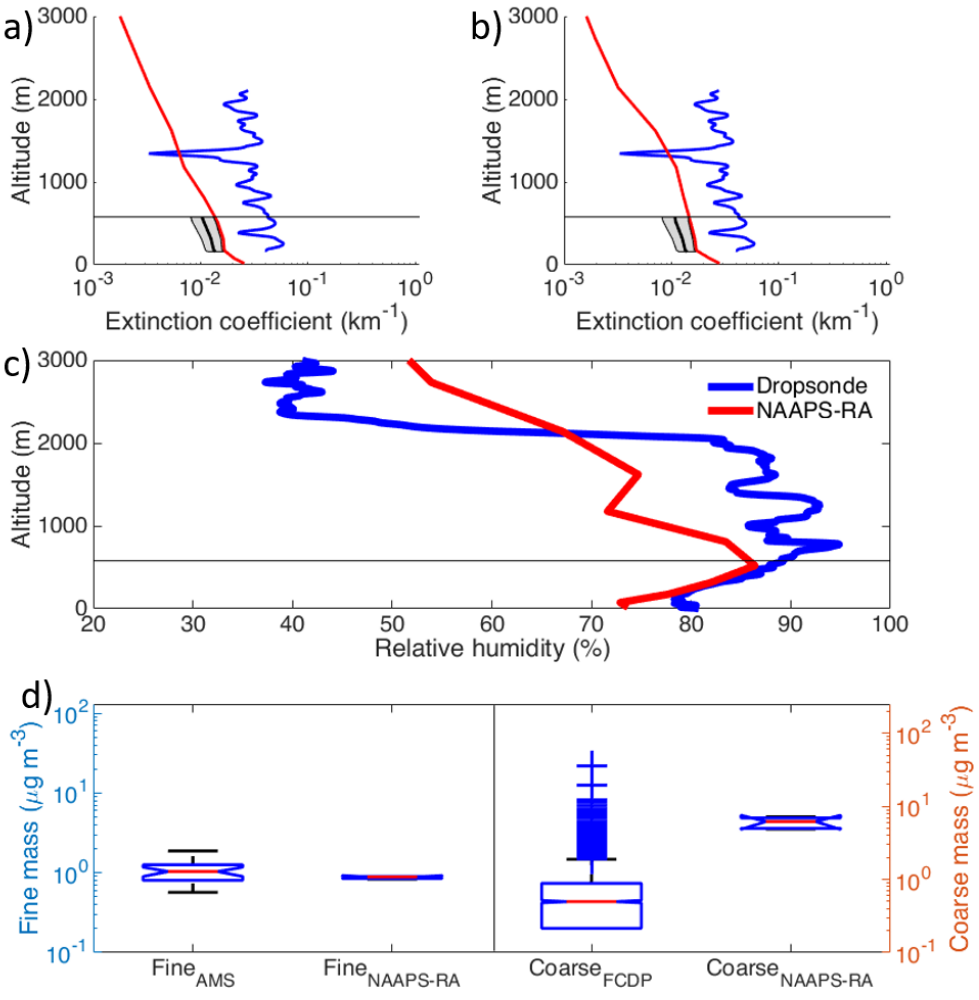

Figure 6. Comparison of model output and observations for the clean case study (RF19) on 5 October 2019. HSRL-2 (blue) and NAAPS-RA extinction profiles (red and black) when NAAPS-RA extinction coefficients were calculated using RH from (**a**) NAAPS-RA and (**b**) dropsonde data. NAAPS-RA extinction coefficients were calculated using either model-defined γ values (red) or the mean in situ γ value (black). Left and right shaded areas extend to NAAPS-RA extinction profiles calculated using γ values one standard deviation below and above the observed mean, respectively. (**c**) Dropsonde and NAAPS-RA RH profiles within the mixed layer (ML). Black horizontal lines denote the mixed layer height (MLH). (**d**) Fine and coarse mass concentrations derived from AMS and FCDP measurements (Sect. 2.9), respectively, as well as those simulated by NAAPS-RA. The red line in the center of each box represents the median, the edges of each box indicate the 25th and 75th quartiles, blue crosses belong to outliers lying in the fourth quartile, and notches represent the 95% confidence interval.

https://doi.org/10.5194/acp-2021-870
Preprint. Discussion started: 30 November 2021


Atmospheric Chemistry and Physics Discussions

3.4.2 Biomass Burning Smoke (RF9)

In contrast to the clean case study, RF9 sampled the most polluted conditions for the campaign as smoke from the MC advected into the Sulu Sea (HSRL-2 AOT and AOT_{ML} ranged from 0.36 – 1.22 and 0.18 – 0.45, respectively). Hilario et al. (2021) found the majority of long range transport from the MC occurs below ~3 km and that a significant fraction occurs below 950 hPa (~800 m), which is similar in altitude to the mean MLH for this case study (633 m). HSRL-2 extinction coefficients increased with altitude in the ML (Fig. 7a), presumably because of increased particle mass concentrations above the surface due to long range transport and/or increased particle hygroscopic growth as RH increased with altitude. NAAPS-RA underestimated extinction by ~12% (b_{ext} bias = -0.09 km^{-1}; HSRL-2 b_{ext} mean = 0.72 ± 0.22 km^{-1}; AOT_{ML} bias = -0.03; AOT bias = -0.11), and simulated a relatively uniform extinction profile throughout the ML that did not resemble the HSRL-2 profile. Modeled fine mode extinction was approximately two orders of magnitude greater than coarse mode extinction throughout the ML (Figs. S11a-b), presumably because NAAPS-RA determined smoke and ABF particles to make up ~80% and ~10%, of the total mass, respectively, (Fig. S11c). Images of aerosol types derived from multiple HSRL-2 products (Burton et al., 2013) supported that smoke was the most prevalent species in the ML (Fig. S12).

When dropsonde RHs were used, NAAPS-RA extinction coefficients increased so that AOT_{ML} and b_{ext} became positively biased (0.05 and 0.01 km^{-1}, respectively; Fig. 7b), which was expected as the model underestimated RH throughout the ML (Fig. 7c). NAAPS-RA also inaccurately modeled particle hygroscopic growth. Negative in situ γ values (-0.06 ± 0.02) implied that a majority of the smoke particles were non-spherical and collapsed into spherical morphology upon humidification (Shingler et al., 2016), which contradicts the small but nevertheless positive γ value NAAPS-RA assigns to smoke particles. Thus, when in situ γ values were used, model extinction decreased and the negative bias for b_{ext} (-0.23 to -0.25 km^{-1}) and AOT_{ML} (-0.18) became larger than that of any other case study. After correcting RHs and γ, the extinction profiles took on the opposite shape of the HSRL-2 profile (i.e., model extinction decreased with altitude), which indicates there were errors in simulated vertical profiles of particle mass concentrations and/or mass extinction efficiency. Specifically, one (or both) of these parameters would need to increase with altitude in order to achieve extinction agreement with the HSRL-2. NAAPS-RA simulated uniform mass fractions in the ML, which implies modeled mass extinction efficiency did not vary with altitude in this 1° grid. Additionally NAAPS-RA simulated low vertical variability for fine and coarse particle mass concentrations (106.41 – 118.36 and 12.08 – 13.06 μg m^{-3}, respectively) within the ML (Fig. 6d). Fine and coarse mass concentrations from the AMS and FCDP exhibited much greater variability (24.16 – 68.57 and 0.11 – 138.16 μg m^{-3}, respectively), although this was predominantly horizontal variability as the aircraft maintained a relatively constant altitude (304.70 – 324.50 m) while flying through the ML in this 1° grid. More work is needed to fully evaluate model simulations of particle mass concentrations and mass extinction efficiency.

https://doi.org/10.5194/acp-2021-870
Preprint. Discussion started: 30 November 2021

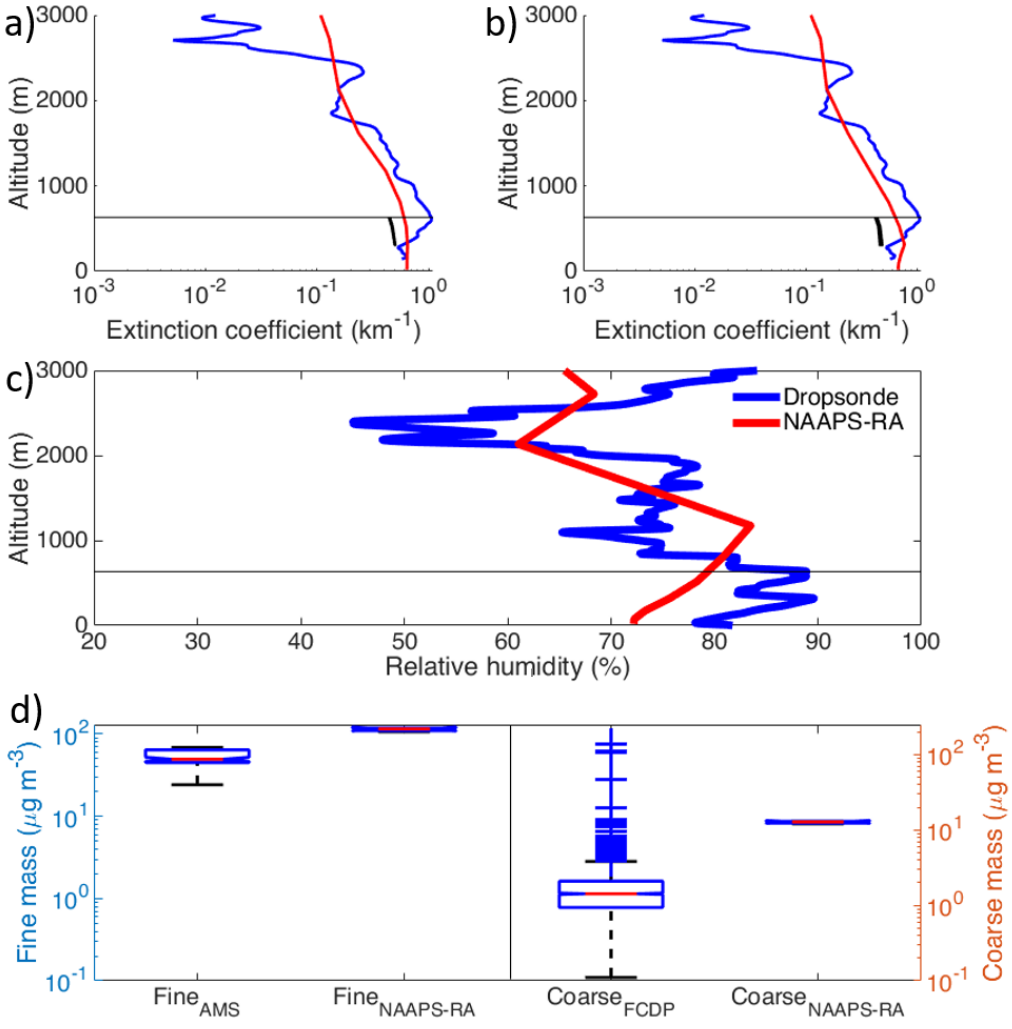

Figure 7. Same as Fig. 6, except for the biomass burning smoke case study (RF9) on 15 September 2019.

https://doi.org/10.5194/acp-2021-870
Preprint. Discussion started: 30 November 2021


Atmospheric Chemistry and Physics Discussions

692 **3.4.3 Asian pollution (RF17)**

693 This case study provided an opportunity to assess model performance for an air mass
694 dominated by urban pollution from Asia (Fig. S13) with moderate AOT (HSRL-2 AOT and
695 AOT_{ML} ranged from 0.10 – 0.34 and 0.03 – 0.10, respectively). Simulated total extinction was
696 dominated by fine mode particles (Figs. S14a-b), presumably because of the significant presence
697 of ABF particles (ABF mass fractions ranged from 0.66 – 0.73; Fig. S14c). ABF is arguably one
698 of the most difficult aerosol types for NAAPS-RA to accurately model as it combines organic
699 and inorganic species, which can have very different hygroscopic and optical properties.
700 NAAPS-RA assigns a γ value to ABF by assuming 40% SO_4^{2-} and 60% OA. However, this
701 composition is likely to vary across different regions, motivating interest in how such an
702 assumption may contribute to model errors in extinction. This case study featured an air mass
703 dominated by ABF, but the mass fractions of SO_4^{2-} and OA (63% and 21%, respectively) were
704 largely different than assigned values from NAAPS-RA (Fig. S15).
705 Originally, NAAPS-RA simulated the opposite extinction profile compared to what was
706 retrieved with the HSRL-2 (Fig. 8a). The model overestimated (underestimated) extinction from
707 ~145 – 250 m (~250 m to the MLH [532 m]), which resulted in an overall negative bias for
708 b_{ext} and AOT_{ML} (-0.02 km^{-1} and -0.02, respectively). NAAPS-RA continued to underestimate
709 extinction above the MLH, and the simulated AOT (0.16) was less than half of the retrieved
710 AOT (0.34). Substituting dropsonde RHs corrected the shape of the profile in the ML (Fig. 8b),
711 suggesting original errors in extinction were driven mainly by errors in modeled RH (Fig. 8c).
712 After substituting dropsonde RHs, NAAPS-RA overestimated extinction (bias = 0.11 km^{-1}),
713 implying the model overestimated either hygroscopic growth for ABF particles or particle mass
714 concentrations (or both). The mean in situ γ value (0.24 ± 0.06) was nearly half the mean
715 NAAPS-RA mass weighted γ (0.42 ± 0.01) and the γ value assigned to ABF (0.46). When in situ
716 γ values were used in the model, extinction agreement improved dramatically and extinction bias
717 (-0.05–0.00 km^{-1}) was closer to zero than for any other case study. This suggests that the γ value
718 assigned to ABF requires modification for this region.
719 Correcting RH and γ yielded excellent extinction agreement below ~250 m, although
720 NAAPS-RA still underestimated extinction from ~250 m to the MLH. Thus, NAAPS-RA
721 underestimated dry mass extinction in the upper half of the ML, which could be for a number of
722 reasons. First, NAAPS-RA may not be modeling mass extinction efficiency correctly in this
723 altitude range. Alternatively, NAAPS-RA may be underestimating particle mass concentrations
724 in the upper half of the ML. The model showed little vertical variability for fine and coarse
725 particle concentrations throughout the ML (20.66 – 25.31 and 8.58 – 10.03 μg m^{-3}, respectively),
726 which was in contrast to the larger ranges for in situ fine and coarse masses (3.86 – 12.13 and 0 –
727 239.80 μg m^{-3}, respectively; Fig. 8d). Although our results suggest NAAPS-RA typically
728 overestimated fine and coarse mass concentrations, there are a few instances when in situ coarse
729 masses were an order of magnitude higher than model simulations. Interestingly, the four highest
730 in situ coarse mass concentrations (105.84, 117.07, 231.03, and 239.80 μg m^{-3}) were all observed
731 from 464 – 500 m. However, RHs were >90% for each of these points, which is the range of RH
732 where our method to derive coarse mass concentrations from FCDP size distributions is subject
733 to the greatest uncertainty. More work is certainly required to understand why NAAPS-RA
734 underestimated extinction above ~250 m for this case study.

https://doi.org/10.5194/acp-2021-870
Preprint. Discussion started: 30 November 2021

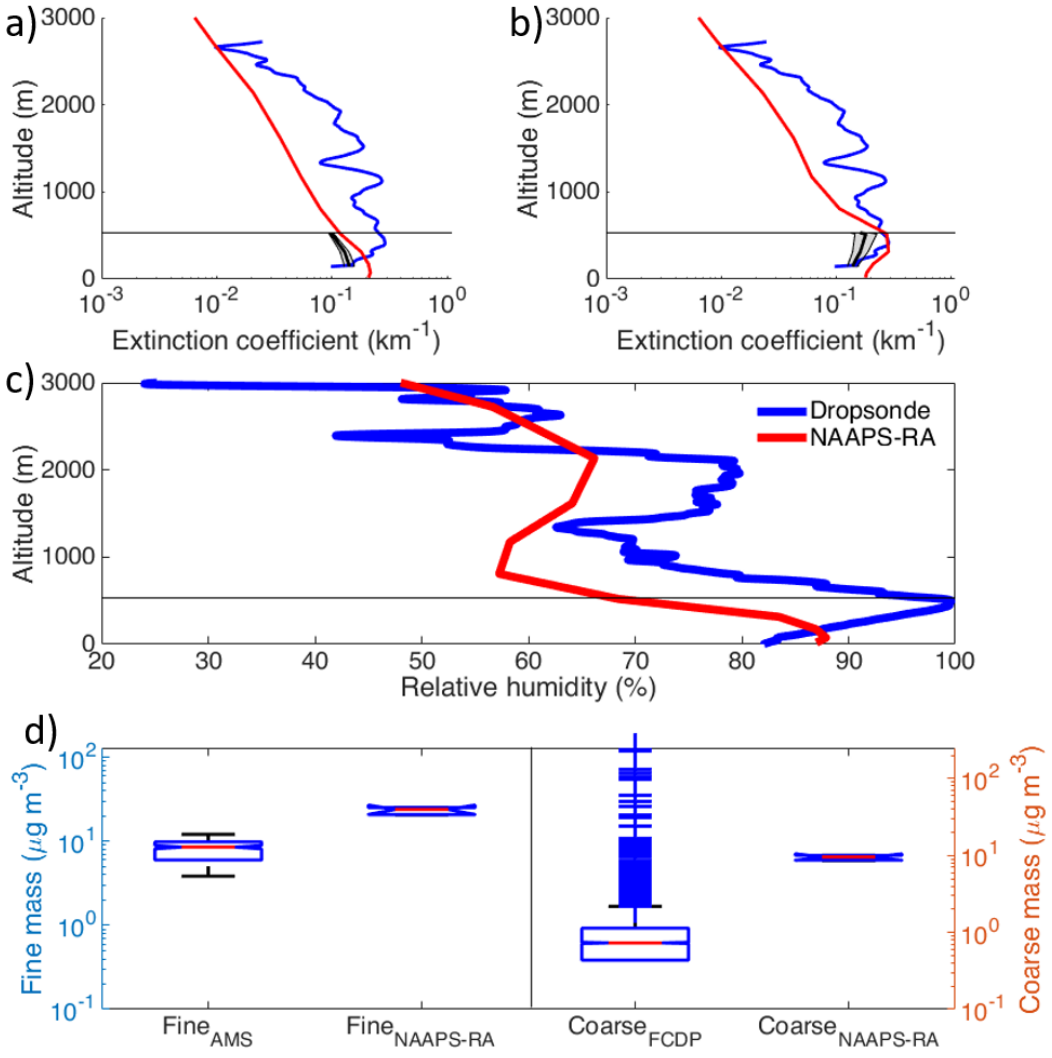

Figure 8. Same as Fig. 6, except for the Asian pollution case study (RF17) on 1 October 2019.

https://doi.org/10.5194/acp-2021-870
Preprint. Discussion started: 30 November 2021


Atmospheric Chemistry and Physics Discussions

737 **3.4.4 Mixed (RF10)**

738 RF10 was noteworthy for the variety of sampled air masses (e.g., volcanic emissions over
739 Mayon, East Asian outflow, aged smoke from the MC) and meteorological conditions (e.g.,
740 outflow boundaries, heavy rainfall, convection), which resulted in a wide range of AOT retrievals
741 (HSRL-2 AOT and AOT_{ML} ranged from 0.16 – 0.62 and 0.06 – 0.22, respectively). Although two
742 air masses converged in the 1° grid selected for this case study, the grid was largely dominated by
743 aged smoke from the MC. This was the same air mass that was sampled during RF9, with the
744 important difference that the smoke had aged an additional ~24 hours (note that the smoke had
745 already aged for a few days before it was sampled during RF9).

746 Simulated total extinction was dominated by fine particles (Figs. S16a-b), which were
747 predominantly smoke particles (Fig. S16c). AMS data indicate the smoke plume sampled during
748 RF9 and RF10 had very similar chemical compositions, yet in situ γ values for RF10 suggest the
749 smoke entering the Philippine Sea was more hygroscopic (γ = 0.04 ± 0.12) than it was in the Sulu
750 Sea during RF9 (γ = -0.06 ± 0.02). However, the hygroscopic properties of this smoke mass are
751 not straightforward as both positive and negative γ values were observed. More work is needed to
752 fully explain this phenomenon. Nonetheless, NAAPS-RA treats all smoke particles the same, no
753 matter their age, motivating interest in how such an assumption could lead to errors in simulated
754 extinction.

755 For this particular case study, NAAPS-RA greatly overestimated AOT, AOT_{ML}, and
756 b_{ext} throughout the ML (biases were 0.54, 0.10, and 0.24 km^{-1}, respectively; Fig. 9a). HSRL-2
757 extinction decreased sharply by an order of magnitude above ~850 m, whereas NAAPS-RA
758 extinction gradually decreased with altitude, which contributed to the large positive bias for AOT.
759 Agreement slightly worsened for AOT_{ML} and b_{ext} (bias = 0.12 and 0.26 km^{-1}, respectively) when
760 dropsonde RHs were used (Fig. 9b) due to underestimated NAAPS-RA RH values, particularly
761 above 300 m (Fig. 9c).

762 Similarly to the smoke case study, the model both overestimated the hygroscopicity of
763 smoke particles and failed to capture the variability in their hygroscopicity (mean simulated and
764 in situ γ values were 0.25 ± 0.00 and 0.04 ± 0.12, respectively). Even after adopting in situ RHs
765 and γ values, NAAPS-RA overestimated extinction (bias = 0.10 – 0.20 km^{-1}) throughout the ML,
766 suggesting there was a positive bias for dry extinction. In situ fine and coarse mass concentrations
767 provide supporting evidence that NAAPS-RA overestimated particle mass in the ML (Fig. 9d).
768 NAAPS-RA may also be overestimating extinction in the ML due to overestimating smoke particle
769 mass extinction efficiency. However, additional research is needed to fully understand why
770 simulated extinction coefficients were so positively biased for this case study (as well as for other
771 locations sampled during RF10).

https://doi.org/10.5194/acp-2021-870
Preprint. Discussion started: 30 November 2021

Atmospheric Chemistry and Physics Discussions

772

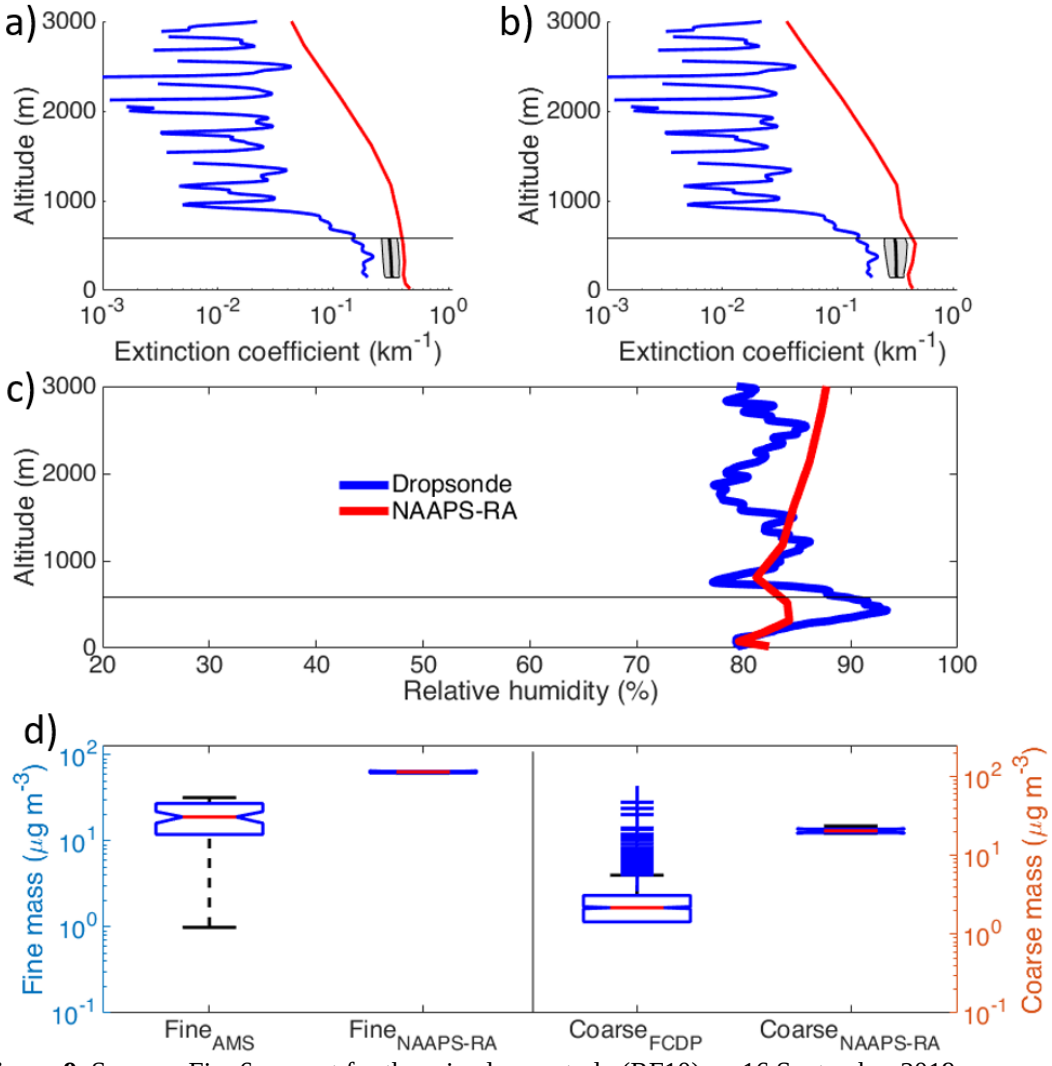

773
774 **Figure 9.** Same as Fig. 6, except for the mixed case study (RF10) on 16 September 2019.

https://doi.org/10.5194/acp-2021-870
Preprint. Discussion started: 30 November 2021

Atmospheric Chemistry and Physics Discussions

4. Conclusions

This study evaluated NAAPS-RA AOT output during the CAMP^{2}Ex field campaign. First, 177 model AOT simulations were compared to collocated AOT retrievals made with a HSRL-2 over the course of 19 research flights. Model and retrieved aerosol extinction coefficients were then compared in three altitude layers to reveal if model performance varied with altitude. Finally, four case studies were analyzed to see how well NAAPS-RA represented (i) RH, (ii) particle hygroscopic growth, and (iii) dry extinction in the ML, and to understand how errors in these parameters affected extinction outputs. The main findings of this work are as follows:

- NAAPS-RA showed AOT correlations of R^2 = 0.68 with the HSRL-2 throughout the campaign. However, modeled AOT was most biased (0.26) during RF10, which sampled a wide range of air masses (e.g., aged smoke advecting into the Philippine Sea, East Asian outflow) as well as complex meteorological conditions (e.g., outflow boundaries, heavy rainfall, convection).
- Aerosol extinction coefficient agreement was best from 145 – 500 m (R^2 = 0.75) and declined with altitude (R^2 = 0.69 and 0.26 for 500 – 1500 m and above 1500 m, respectively). Agreement did not improve when dropsonde RH values were substituted into the model, presumably because of error cancellations and issues in how NAAPS-RA simultaneously modeled other parameters (e.g., particle hygroscopicity, particle mass concentrations, mass extinction efficiencies).
- NAAPS-RA showed poor RH correlation (R^2 = 0.49) with dropsonde measurements and underestimated RH at all altitudes, especially below 500 m (bias = -4.9%) and between 500 and 1500 m (bias = -7.7%).
- The model overestimated the hygroscopic growth parameter, γ, for (i) aged smoke particles transported from the MC, and (ii) anthropogenic and biogenic fine (ABF) particles in an air mass dominated by East Asian outflow.

Findings from this work can assist the modeling community to improve AOT forecasts in SEA and beyond. For example, our results reveal NAAPS-RA overestimated the hygroscopicity of particles from biomass burning in the MC as well as anthropogenic particles transported from East Asia, which led to inaccurate extinction outputs. This result may apply to other smoke plumes and/or urban environments, motivating future works to examine model performance in these types of air masses elsewhere.

Data Availability

The CAMP^{2}Ex dataset can be found at https://doi.org/10.5067//Suborbital/CAMP2EX2018/DATA001; NAAPS-RA AOT data are available at https://usgodae.org/cgi-bin/datalist.pl?dset=nrl_naaps_reanalysis&summary=Go.

Author Contributions

JSR, PX, SPB, ALC, ECC, MAF, RAF, SWF, JWH, DBH, CAH, CER, AJS, MAS, GAS, SCvdH, ELW, SW, and LDZ collected and/or prepared the data. EE conducted the data analysis. EE, AS, JSR, and PX conducted data interpretation. EE and AS prepared the manuscript with editing from all coauthors.

Competing Interests

https://doi.org/10.5194/acp-2021-870
Preprint. Discussion started: 30 November 2021


Atmospheric Chemistry and Physics Discussions

821 The authors declare that they have no conflict of interest.
822
823 **Acknowledgements**
824 The authors acknowledge those involved with executing the CAMP^{2}Ex campaign. The
825 authors also acknowledge Office of Naval Research code 322, the NASA Interdisciplinary Science
826 Program, the NRL Base Program, and the Office of Naval Research 35 for the development of
827 NAAPS reanalysis. EE acknowledges support from the Naval Research Enterprise Internship
828 Program (NREIP).
829
830 **Financial Support**
831 CAMP^{2}Ex measurements and data analysis were funded by NASA grant
832 80NSSC18K0148. This work was also partially supported by ONR grant N00014-21-1-2115 and
833 NASA grant 80NSSC19K0442 in support of the ACTIVATE Earth Venture Suborbital-3 (EVS-
834 3) investigation, which is funded by NASA's Earth Science Division and managed through the
835 Earth System Science Pathfinder Program Office.
836

https://doi.org/10.5194/acp-2021-870
Preprint. Discussion started: 30 November 2021

Atmospheric Chemistry and Physics Discussions

References

Adler, R. F., Kidd, C., Petty, G., Morissey, M., and Goodman, H. M.: Intercomparison of Global Precipitation Products: The Third Precipitation Intercomparison Project (PIP–3), Bulletin of the American Meteorological Society, 82, 1377-1396, https://doi.org/10.1175/1520-0477(2001)082<1377:iogppt>2.3.co;2, 2001.

Alas, H. D., Müller, T., Birmili, W., Kecorius, S., Cambaliza, M. O., Simpas, J. B. B., Cayetano, M., Weinhold, K., Vallar, E., Galvez, M. C., and Wiedensohler, A.: Spatial Characterization of Black Carbon Mass Concentration in the Atmosphere of a Southeast Asian Megacity: An Air Quality Case Study for Metro Manila, Philippines, Aerosol and Air Quality Research, 18, 2301-2317, https://doi.org/10.4209/aaqr.2017.08.0281, 2018.

Anderson, T. L. and Ogren, J. A.: Determining Aerosol Radiative Properties Using the TSI 3563 Integrating Nephelometer, Aerosol Science and Technology, 29, 57-69, https://doi.org/10.1080/02786829808965551, 1998.

Atwood, S. A., Reid, J. S., Kreidenweis, S. M., Blake, D. R., Jonsson, H. H., Lagrosas, N. D., Xian, P., Reid, E. A., Sessions, W. R., and Simpas, J. B.: Size-resolved aerosol and cloud condensation nuclei (CCN) properties in the remote marine South China Sea – Part 1: Observations and source classification, Atmospheric Chemistry and Physics, 17, 1105-1123, https://doi.org/10.5194/acp-17-1105-2017, 2017.

Azadiaghdam, M., Braun, R. A., Edwards, E.-L., Bañaga, P. A., Cruz, M. T., Betito, G., Cambaliza, M. O., Dadashazar, H., Lorenzo, G. R., Ma, L., Macdonald, A. B., Nguyen, P., Simpas, J. B., Stahl, C., and Sorooshian, A.: On the nature of sea salt aerosol at a coastal megacity: Insights from Manila, Philippines in Southeast Asia, Atmospheric Environment, 216, 116922, https://doi.org/10.1016/j.atmosenv.2019.116922, 2019.

Betts, A. K. and Albrecht, B. A.: Conserved Variable Analysis of the Convective Boundary Layer Thermodynamic Structure over the Tropical Oceans, Journal of the Atmospheric Sciences, 44, 83-99, https://doi.org/10.1175/1520-0469(1987)044<0083:cvaotc>2.0.co;2, 1987.

Beyersdorf, A. J., Ziemba, L. D., Chen, G., Corr, C. A., Crawford, J. H., Diskin, G. S., Moore, R. H., Thornhill, K. L., Winstead, E. L., and Anderson, B. E.: The impacts of aerosol loading, composition, and water uptake on aerosol extinction variability in the Baltimore–Washington, D.C. region, Atmospheric Chemistry and Physics, 16, 1003-1015, https://doi.org/10.5194/acp-16-1003-2016, 2016.

Burkart, J., Steiner, G., Reischl, G., Moshammer, H., Neuberger, M., and Hitzenberger, R.: Characterizing the performance of two optical particle counters (Grimm OPC1.108 and OPC1.109) under urban aerosol conditions, Journal of Aerosol Science, 41, 953-962, https://dx.doi.org/10.1016/j.jaerosci.2010.07.007, 2010.

Burton, S. P., Ferrare, R. A., Vaughan, M. A., Omar, A. H., Rogers, R. R., Hostetler, C. A., and Hair, J. W.: Aerosol classification from airborne HSRL and comparisons with the CALIPSO vertical feature mask, Atmospheric Measurement Techniques, 6, 1397-1412, https://dx.doi.org/10.5194/amt-6-1397-2013, 2013.

Burton, S. P., Hostetler, C. A., Cook, A. L., Hair, J. W., Seaman, S. T., Scola, S., Harper, D. B., Smith, J. A., Fenn, M. A., Ferrare, R. A., Saide, P. E., Chemyakin, E. V., and Müller, D.: Calibration of a high spectral resolution lidar using a Michelson interferometer, with data examples from ORACLES, Appl. Opt., 57, 6061, https://dx.doi.org/10.1364/ao.57.006061, 2018.

https://doi.org/10.5194/acp-2021-870
Preprint. Discussion started: 30 November 2021

Atmospheric Chemistry and Physics Discussions

883 Campbell, J. R., Reid, J. S., Westphal, D. L., Zhang, J., Tackett, J. L., Chew, B. N., Welton, E. J.,
884 Shimizu, A., Sugimoto, N., Aoki, K., and Winker, D. M.: Characterizing the vertical
885 profile of aerosol particle extinction and linear depolarization over Southeast Asia and the
886 Maritime Continent: The 2007–2009 view from CALIOP, Atmospheric Research, 122,
887 520-543, https://doi.org/10.1016/j.atmosres.2012.05.007, 2013.
888 Canagaratna, M. R., Jayne, J. T., Jimenez, J. L., Allan, J. D., Alfarra, M. R., Zhang, Q., Onasch,
889 T. B., Drewnick, F., Coe, H., Middlebrook, A., Delia, A., Williams, L. R., Trimborn, A.
890 M., Northway, M. J., Decarlo, P. F., Kolb, C. E., Davidovits, P., and Worsnop, D. R.:
891 Chemical and microphysical characterization of ambient aerosols with the aerodyne
892 aerosol mass spectrometer, Mass Spectrometry Reviews, 26, 185-222,
893 https://doi.org/10.1002/mas.20115, 2007.
894 Cinco, T. A., De Guzman, R. G., Hilario, F. D., and Wilson, D. M.: Long-term trends and
895 extremes in observed daily precipitation and near surface air temperature in the
896 Philippines for the period 1951–2010, Atmospheric Research, 145-146, 12-26,
897 https://doi.org/10.1016/j.atmosres.2014.03.025, 2014.
898 Colarco, P., Da Silva, A., Chin, M., and Diehl, T.: Online simulations of global aerosol
899 distributions in the NASA GEOS-4 model and comparisons to satellite and ground-based
900 aerosol optical depth, Journal of Geophysical Research, 115,
901 https://doi.org/10.1029/2009jd012820, 2010.
902 Cruz, F., Narisma, G., Villafuerte Ii, M., Chua, K. U., and Olaguera, L. M.: A climatological
903 analysis of the southwest monsoon rainfall in the Philippines, Atmospheric Research,
904 122, 609–616, https://doi.org/10.1016/j.atmosres.2012.06.010, 2013.
905 Cruz, M. T., Bañaga, P. A., Betito, G., Braun, R. A., Stahl, C., Aghdam, M. A., Cambaliza, M.
906 O., Dadashazar, H., Hilario, M. R., Lorenzo, G. R., Ma, L., Macdonald, A. B., Pabroa, P.
907 C., Yee, J. R., Simpas, J. B., and Sorooshian, A.: Size-resolved composition and
908 morphology of particulate matter during the southwest monsoon in Metro Manila,
909 Philippines, Atmospheric Chemistry and Physics, 19, 10675-10696,
910 https://doi.org/10.5194/acp-19-10675-2019, 2019.
911 Dai, A.: Precipitation Characteristics in Eighteen Coupled Climate Models, Journal of Climate,
912 19, 4605-4630, https://doi.org/10.1175/jcli3884.1, 2006.
913 Decarlo, P. F., Kimmel, J. R., Trimborn, A., Northway, M. J., Jayne, J. T., Aiken, A. C., Gonin,
914 M., Fuhrer, K., Horvath, T., Docherty, K. S., Worsnop, D. R., and Jimenez, J. L.: Field-
915 Deployable, High-Resolution, Time-of-Flight Aerosol Mass Spectrometer, Analytical
916 Chemistry, 78, 8281-8289, https://doi.org/10.1021/ac061249n, 2006.
917 Fast, J. D., Gustafson, W. I., Chapman, E. G., Easter, R. C., Rishel, J. P., Zaveri, R. A., Grell, G.
918 A., and Barth, M. C.: The Aerosol Modeling Testbed: A Community Tool to Objectively
919 Evaluate Aerosol Process Modules, Bulletin of the American Meteorological Society, 92,
920 343-360, https://doi.org/10.1175/2010bams2868.1, 2011.
921 Fast, J. D., Gustafson Jr, W. I., Berg, L. K., Shaw, W. J., Pekour, M., Shrivastava, M., Barnard,
922 J. C., Ferrare, R. A., Hostetler, C. A., Hair, J. A., Erickson, M., Jobson, B. T., Flowers,
923 B., Dubey, M. K., Springston, S., Pierce, R. B., Dolislager, L., Pederson, J., and Zaveri,
924 R. A.: Transport and mixing patterns over Central California during the carbonaceous
925 aerosol and radiative effects study (CARES), Atmospheric Chemistry and Physics, 12,
926 1759-1783, https://doi.org/10.5194/acp-12-1759-2012, 2012.
927 Gelaro, R., McCarty, W., Suárez, M. J., Todling, R., Molod, A., Takacs, L., Randles, C. A.,
928 Darmenov, A., Bosilovich, M. G., Reichle, R., Wargan, K., Coy, L., Cullather, R.,

Draper, C., Akella, S., Buchard, V., Conaty, A., Da Silva, A. M., Gu, W., Kim, G.-K., Koster, R., Lucchesi, R., Merkova, D., Nielsen, J. E., Partyka, G., Pawson, S., Putman, W., Rienecker, M., Schubert, S. D., Sienkiewicz, M., and Zhao, B.: The Modern-Era Retrospective Analysis for Research and Applications, Version 2 (MERRA-2), Journal of Climate, 30, 5419-5454, https://doi.org/10.1175/jcli-d-16-0758.1, 2017.

Glienke, S. and Mei, F.: Fast cloud droplet probe (FCDP) instrument handbook, ARM Data Center, Oak Ridge National Laboratory (ORNL), Oak Ridge, TN (United …, 2020.

Gordon, H. R.: Atmospheric Correction of Ocean Color Imagery in the Earth Observing System Era, Journal of Geophysical Research, 102D, 17081-17106, https://doi.org/10.1029/96JD02443, 1997.

Groß, S., Esselborn, M., Weinzierl, B., Wirth, M., Fix, A., and Petzold, A.: Aerosol classification by airborne high spectral resolution lidar observations, Atmospheric Chemistry and Physics, 13, 2487-2505, https://doi.org/10.5194/acp-13-2487-2013, 2013.

Gupta, P., Christopher, S. A., Wang, J., Gehrig, R., Lee, Y., and Kumar, N.: Satellite remote sensing of particulate matter and air quality assessment over global cities, Atmospheric Environment, 40, 5880-5892, https://doi.org/10.1016/j.atmosenv.2006.03.016, 2006.

Hair, J. W., Hostetler, C. A., Cook, A. L., Harper, D. B., Ferrare, R. A., Mack, T. L., Welch, W., Izquierdo, L. R., and Hovis, F. E.: Airborne High Spectral Resolution Lidar for profiling aerosol optical properties, Appl. Opt., 47, 6734-6752, https://doi.org/10.1364/AO.47.006734, 2008.

Hänel, G.: The Properties of Atmospheric Aerosol Particles as Functions of the Relative Humidity at Thermodynamic Equilibrium with the Surrounding Moist Air, in, Elsevier, 73-188, https://doi.org/10.1016/s0065-2687(08)60142-9, 1976.

Hilario, M. R. A., Cruz, M. T., Cambaliza, M. O. L., Reid, J. S., Xian, P., Simpas, J. B., Lagrosas, N. D., Uy, S. N. Y., Cliff, S., and Zhao, Y.: Investigating size-segregated sources of elemental composition of particulate matter in the South China Sea during the 2011 Vasco cruise, Atmospheric Chemistry and Physics, 20, 1255-1276, https://doi.org/10.5194/acp-20-1255-2020, 2020a.

Hilario, M. R. A., Cruz, M. T., Bañaga, P. A., Betito, G., Braun, R. A., Stahl, C., Cambaliza, M. O., Lorenzo, G. R., Macdonald, A. B., Azadiaghdam, M., Pabroa, P. C., Yee, J. R., Simpas, J. B., and Sorooshian, A.: Characterizing Weekly Cycles of Particulate Matter in a Coastal Megacity: The Importance of a Seasonal, Size-Resolved, and Chemically Speciated Analysis, Journal of Geophysical Research: Atmospheres, 125, https://doi.org/10.1029/2020jd032614, 2020b.

Hilario, M. R. A., Crosbie, E., Shook, M., Reid, J. S., Cambaliza, M. O. L., Simpas, J. B. B., Ziemba, L., Digangi, J. P., Diskin, G. S., Nguyen, P., Turk, F. J., Winstead, E., Robinson, C. E., Wang, J., Zhang, J., Wang, Y., Yoon, S., Flynn, J., Alvarez, S. L., Behrangi, A., and Sorooshian, A.: Measurement report: Long-range transport patterns into the tropical northwest Pacific during the CAMP2Ex aircraft campaign: chemical composition, size distributions, and the impact of convection, Atmospheric Chemistry and Physics, 21, 3777-3802, https://doi.org/10.5194/acp-21-3777-2021, 2021.

Hogan, T. F., Liu, M., Ridout, J. A., Peng, M. S., Whitcomb, T. R., Ruston, B. C., Reynolds, C. A., Eckermann, S. D., Moskaitis, J. R., Baker, N. L., McCormack, J. P., Viner, K. C., McLay, J. G., Flatau, M. K., L. Xu, C. C., and Chang, S. W.: The Navy Global Environmental Model, Oceanography, 27, 116-125, https://doi.org/10.5670/oceanog.2014.73, 2014.

https://doi.org/10.5194/acp-2021-870
Preprint. Discussion started: 30 November 2021


Atmospheric Chemistry and Physics Discussions

975 Hyer, E. J. and Chew, B. N.: Aerosol transport model evaluation of an extreme smoke episode in
976 Southeast Asia, Atmospheric Environment, 44, 1422-1427,
977 https://doi.org/10.1016/j.atmosenv.2010.01.043, 2010.
978 Hyer, E. J., Reid, J. S., and Zhang, J.: An over-land aerosol optical depth data set for data
979 assimilation by filtering, correction, and aggregation of MODIS Collection 5 optical
980 depth retrievals, Atmos. Meas. Tech., 4, 379-408, https://doi.org/10.5194/amt-4-379-
981 2011, 2011.
982 Inness, A., Ades, M., Agustí-Panareda, A., Barré, J., Benedictow, A., Blechschmidt, A.-M.,
983 Dominguez, J. J., Engelen, R., Eskes, H., Flemming, J., Huijnen, V., Jones, L., Kipling,
984 Z., Massart, S., Parrington, M., Peuch, V.-H., Razinger, M., Remy, S., Schulz, M., and
985 Suttie, M.: The CAMS reanalysis of atmospheric composition, Atmospheric Chemistry
986 and Physics, 19, 3515-3556, https://doi.org/10.5194/acp-19-3515-2019, 2019.
987 IPCC: Climate Change 2007. Synthesis Report. Contribution of Working Groups I, II & III to the
988 Fourth Assessment Report of the Intergovernmental Panel on Climate Change. Geneva,
989 in, edited by: Lemke, P., Ren, J. F., Alley, R., Allison, I., Carrasco, J., Flato, G., Fujii, Y.,
990 Kaser, G., Mote, P., Thomas, R., and Zhang, T.,
991 https://doi.org/10.1017/CBO9780511546013, 2007.
992 IPCC: Climate change 2013: The Physical Science Basis. Contribution of Working Group I to
993 the Fifth Assessment Report of the Intergovernmental Panel on Climate Change. Stocker,
994 T.F., D. Qin, G. K. Plattner, M. Tignor, S.K. Allen, J. Boschung, A. Nauels, Y Xia, V.
995 Bex, and P.M. Midgley (eds.), Cambridge University Press, Cambridge, United Kingdom
996 and New York, NY, USA, 1535, https://doi.org/10.1017/CB09781107415324, 2013.
997 Kaku, K. C., Reid, J. S., Hand, J. L., Edgerton, E. S., Holben, B. N., Zhang, J., and Holz, R. E.:
998 Assessing the Challenges of Surface-Level Aerosol Mass Estimates From Remote
999 Sensing During the SEAC 4 RS and SEARCH Campaigns: Baseline Surface
1000 Observations and Remote Sensing in the Southeastern United States, Journal of
1001 Geophysical Research: Atmospheres, 123, 7530-7562,
1002 https://doi.org/10.1029/2017jd028074, 2018.
1003 Kassianov, E., Ovchinnikov, M., Berg, L. K., McFarlane, S. A., Flynn, C., Ferrare, R., Hostetler,
1004 C., and Alexandrov, M.: Retrieval of aerosol optical depth in vicinity of broken clouds
1005 from reflectance ratios: case study, Atmospheric Measurement Techniques, 3, 1333-
1006 1349, https://doi.org/10.5194/amt-3-1333-2010, 2010.
1007 Kecorius, S., Madueño, L., Vallar, E., Alas, H., Betito, G., Birmili, W., Cambaliza, M. O.,
1008 Catipay, G., Gonzaga-Cayetano, M., Galvez, M. C., Lorenzo, G., Müller, T., Simpas, J.
1009 B., Tamayo, E. G., and Wiedensohler, A.: Aerosol particle mixing state, refractory
1010 particle number size distributions and emission factors in a polluted urban environment:
1011 Case study of Metro Manila, Philippines, Atmospheric Environment, 170, 169-183,
1012 https://doi.org/10.1016/j.atmosenv.2017.09.037, 2017.
1013 Knobelspiesse, K., Cairns, B., Redemann, J., Bergstrom, R. W., and Stohl, A.: Simultaneous
1014 retrieval of aerosol and cloud properties during the MILAGRO field campaign,
1015 Atmospheric Chemistry and Physics, 11, 6245-6263, https://doi.org/10.5194/acp-11-
1016 6245-2011, 2011.
1017 Knutson, T., Camargo, S. J., Chan, J. C. L., Emanuel, K., Ho, C.-H., Kossin, J., Mohapatra, M.,
1018 Satoh, M., Sugi, M., Walsh, K., and Wu, L.: Tropical Cyclones and Climate Change
1019 Assessment: Part I: Detection and Attribution, Bulletin of the American Meteorological
1020 Society, 100, 1987-2007, https://doi.org/10.1175/BAMS-D-18-0189.1, 2019.

1021 Kulkarni, P. and Baron, P. A.: An Approach to Performing Aerosol Measurements. In Aerosol
1022 Measurements, https://doi.org/10.1002/9781118001684.ch5, 2011.
1023 Lagmay, A. M. F., Agaton, R. P., Bahala, M. A. C., Briones, J. B. L. T., Cabacaba, K. M. C.,
1024 Caro, C. V. C., Dasallas, L. L., Gonzalo, L. A. L., Ladiero, C. N., Lapidez, J. P.,
1025 Mungcal, M. T. F., Puno, J. V. R., Ramos, M. M. A. C., Santiago, J., Suarez, J. K., and
1026 Tablazon, J. P.: Devastating storm surges of Typhoon Haiyan, International Journal of
1027 Disaster Risk Reduction, 11, 1-12, https://doi.org/10.1016/j.ijdrr.2014.10.006, 2015.
1028 Lewis, E. R. and Schwartz, S. E.: Sea Salt Aerosol Production: Mechanisms, Methods,
1029 Measurements and Models American Geophysical Union, Washington, DC,
1030 https://doi.org/10.1002/9781118666050.ch2, 2004.
1031 Li, J., Chu, Y., Li, X., and Dong, Y.: Long-term trends of global maximum atmospheric mixed
1032 layer heights derived from radiosonde measurements, Environmental Research Letters,
1033 15, 034054, https://doi.org/10.1088/1748-9326/ab7952, 2020.
1034 Lim, S., Lee, M., Kim, S.-W., and Laj, P.: Sulfate alters aerosol absorption properties in East
1035 Asian outflow, Scientific Reports, 8, https://doi.org/10.1038/s41598-018-23021-1, 2018.
1036 Liu, Y., Franklin, M., Kahn, R., and Koutrakis, P.: Using aerosol optical thickness to predict
1037 ground-level PM2.5 concentrations in the St. Louis area: A comparison between MISR
1038 and MODIS, Remote Sensing of Environment, 107, 33-44,
1039 https://doi.org/10.1016/j.rse.2006.05.022, 2007.
1040 Lynch, P., Reid, J. S., Westphal, D. L., Zhang, J., Hogan, T. F., Hyer, E. J., Curtis, C. A., Hegg,
1041 D. A., Shi, Y., Campbell, J. R., Rubin, J. I., Sessions, W. R., Turk, F. J., and Walker, A.
1042 L.: An 11-year global gridded aerosol optical thickness reanalysis (v1.0) for atmospheric
1043 and climate sciences, Geosci. Model Dev., 9, 1489-1522, https://doi.org/10.5194/gmd-9-
1044 1489-2016, 2016.
1045 Mahmud, M. and Ross, R. S.: Precipitation assessment of a superensemble forecast over South-
1046 East Asia, Meteorological Applications, 12, 177-186,
1047 https://doi.org/10.1017/s1350482705001660, 2005.
1048 May, D. A., Stowe, L. L., Hawkins, J. D., and McClain, E. P.: A correction for Saharan dust
1049 effects on satellite sea-surface temperature-measurements, Journal of Geophysical
1050 Research, 97, 3611-3619, https://doi.org/10.1029/91JC02987, 1992.
1051 McNaughton, C. S., Clarke, A. D., Howell, S. G., Pinkerton, M., Anderson, B., Thornhill, L.,
1052 Hudgins, C., Winstead, E., Dibb, J. E., Scheuer, E., and Maring, H.: Results from the DC-
1053 8 Inlet Characterization Experiment (DICE): Airborne Versus Surface Sampling of
1054 Mineral Dust and Sea Salt Aerosols, Aerosol Science and Technology, 41, 136-159,
1055 https://doi.org/10.1080/02786820601118406, 2007.
1056 Middlebrook, A. M., Bahreini, R., Jimenez, J. L., and Canagaratna, M. R.: Evaluation of
1057 Composition-Dependent Collection Efficiencies for the Aerodyne Aerosol Mass
1058 Spectrometer using Field Data, Aerosol Science and Technology, 46, 258-271,
1059 https://doi.org/10.1080/02786826.2011.620041, 2012.
1060 Prabhakar, G., Ervens, B., Wang, Z., Maudlin, L. C., Coggon, M. M., Jonsson, H. H., Seinfeld, J.
1061 H., and Sorooshian, A.: Sources of nitrate in stratocumulus cloud water: Airborne
1062 measurements during the 2011 E-PEACE and 2013 NiCE studies, Atmospheric
1063 Environment, 97, 166-173, https://doi.org/10.1016/j.atmosenv.2014.08.019, 2014.
1064 Randles, C. A., Da Silva, A. M., Buchard, V., Colarco, P. R., Darmenov, A., Govindaraju, R.,
1065 Smirnov, A., Holben, B., Ferrare, R., Hair, J., Shinozuka, Y., and Flynn, C. J.: The
1066 MERRA-2 Aerosol Reanalysis, 1980 Onward. Part I: System Description and Data

Assimilation Evaluation, Journal of Climate, 30, 6823-6850, https://doi.org/10.1175/jcli-d-16-0609.1, 2017.

Reid, J. S., Xian, P., Hyer, E. J., Flatau, M. K., Ramirez, E. M., Turk, F. J., Sampson, C. R., Zhang, C., Fukada, E. M., and Maloney, E. D.: Multi-scale meteorological conceptual analysis of observed active fire hotspot activity and smoke optical depth in the Maritime Continent, Atmospheric Chemistry and Physics, 12, 2117-2147, https://doi.org/10.5194/acp-12-2117-2012, 2012.

Reid, J. S., Kuehn, R. E., Holz, R. E., Eloranta, E. W., Kaku, K. C., Kuang, S., Newchurch, M. J., Thompson, A. M., Trepte, C. R., Zhang, J., Atwood, S. A., Hand, J. L., Holben, B. N., Minnis, P., and Posselt, D. J.: Ground-based High Spectral Resolution Lidar observation of aerosol vertical distribution in the summertime Southeast United States, Journal of Geophysical Research: Atmospheres, 122, 2970-3004, https://doi.org/10.1002/2016jd025798, 2017.

Reid, J. S., Xian, P., Holben, B. N., Hyer, E. J., Reid, E. A., Salinas, S. V., Zhang, J., Campbell, J. R., Chew, B. N., Holz, R. E., Kuciauskas, A. P., Lagrosas, N., Posselt, D. J., Sampson, C. R., Walker, A. L., Welton, E. J., and Zhang, C.: Aerosol meteorology of the Maritime Continent for the 2012 7SEAS southwest monsoon intensive study – Part 1: regional-scale phenomena, Atmospheric Chemistry and Physics, 16, 14041-14056, https://doi.org/10.5194/acp-16-14041-2016, 2016a.

Reid, J. S., Lagrosas, N. D., Jonsson, H. H., Reid, E. A., Sessions, W. R., Simpas, J. B., Uy, S. N., Boyd, T. J., Atwood, S. A., Blake, D. R., Campbell, J. R., Cliff, S. S., Holben, B. N., Holz, R. E., Hyer, E. J., Lynch, P., Meinardi, S., Posselt, D. J., Richardson, K. A., Salinas, S. V., Smirnov, A., Wang, Q., Yu, L., and Zhang, J.: Observations of the temporal variability in aerosol properties and their relationships to meteorology in the summer monsoonal South China Sea/East Sea: the scale-dependent role of monsoonal flows, the Madden–Julian Oscillation, tropical cyclones, squall lines and cold pools, Atmos. Chem. Phys., 15, 1745-1768, https://doi.org/10.5194/acp-15-1745-2015, 2015.

Reid, J. S., Hyer, E. J., Johnson, R. S., Holben, B. N., Yokelson, R. J., Zhang, J., Campbell, J. R., Christopher, S. A., Di Girolamo, L., Giglio, L., Holz, R. E., Kearney, C., Miettinen, J., Reid, E. A., Turk, F. J., Wang, J., Xian, P., Zhao, G., Balasubramanian, R., Chew, B. N., Janjai, S., Lagrosas, N., Lestari, P., Lin, N.-H., Mahmud, M., Nguyen, A. X., Norris, B., Oanh, N. T. K., Oo, M., Salinas, S. V., Welton, E. J., and Liew, S. C.: Observing and understanding the Southeast Asian aerosol system by remote sensing: An initial review and analysis for the Seven Southeast Asian Studies (7SEAS) program, Atmospheric Research, 122, 403-468, https://doi.org/10.1016/j.atmosres.2012.06.005, 2013.

Reid, J. S., Lagrosas, N. D., Jonsson, H. H., Reid, E. A., Atwood, S. A., Boyd, T. J., Ghate, V. P., Xian, P., Posselt, D. J., Simpas, J. B., Uy, S. N., Zaiger, K., Blake, D. R., Bucholtz, A., Campbell, J. R., Chew, B. N., Cliff, S. S., Holben, B. N., Holz, R. E., Hyer, E. J., Kreidenweis, S. M., Kuciauskas, A. P., Lolli, S., Oo, M., Perry, K. D., Salinas, S. V., Sessions, W. R., Smirnov, A., Walker, A. L., Wang, Q., Yu, L., Zhang, J., and Zhao, Y.: Aerosol meteorology of Maritime Continent for the 2012 7SEAS southwest monsoon intensive study – Part 2: Philippine receptor observations of fine-scale aerosol behavior, Atmospheric Chemistry and Physics, 16, 14057-14078, https://doi.org/10.5194/acp-16-14057-2016, 2016b.

Reid, J. S., Maring, H., Thompson, E., Ziemba, L., Mace, J., di Girolamo, L., Simpas, J. B., Cambaliza, M. O., Lawson, R. P., Tanelli, S., Sy, O., Lang, T., van den Heever, S.,

Ferrare, R., van Diedenhoven, B., Holz, R., Kowch, R., Schmidt, S., Collow, A., Bucholtz, A., Smith, G., Sorooshian, A., Wang, J., diskin, G., Yoon, S.-C., Thornhill, K. L., Montes, M., Eleuterio, D. P., Roelof, B., Woods, S., Douthett, C., Sekiyama, T., Taichu, T., Brooks, M. E., Bendetti, A., Nowottnick, E., Xian, P., Kuehn, R. E., Zavaleta, J., Hristova-Veleva, S., Trepte, C., Freeman, S., Canyanan, E., Chen, G., Shook, M., Amiot, C., Crosbie, E., Burton, S. P., Hostetler, C., Leung, G., Rutledge, S., Moum, J., and Shroyer, E.: The coupling between tropical meteorology, aerosol science, convection and the energy budget during the Clouds, Aerosol Monsoon Processes Philippines Experiment (CAMP2Ex), Bulletin of the American Meteorological Society, 2021 (in preparation).

Retalis, A., Hadjimitsis, D. G., Michaelides, S., Tymvios, F., Chrysoulakis, N., Clayton, C. R. I., and Themistocleous, K.: Comparison of aerosol optical thickness with in situ visibility data over Cyprus, Natural Hazards and Earth System Sciences, 10, 421-428, https://doi.org/10.5194/nhess-10-421-2010, 2010.

Reynolds, R. W., Folland, C. K., and Parker, D. E.: Biases in satellite-derived sea-surface-temperature data, Nature, 341, 728-731, https://doi.org/10.1038/341728a0, 1989.

Robock, A.: Satellite data contamination, Nature, 341, 695-695, https://doi.org/10.1038/341695a0, 1989.

Ross, A. D., Holz, R. E., Quinn, G., Reid, J. S., Xian, P., Turk, F. J., and Posselt, D. J.: Exploring the first aerosol indirect effect over Southeast Asia using a 10-year collocated MODIS, CALIOP, and model dataset, Atmospheric Chemistry and Physics, 18, 12747-12764, https://doi.org/10.5194/acp-18-12747-2018, 2018.

Rubin, J. I., Reid, J. S., Hansen, J. A., Anderson, J. L., Collins, N., Hoar, T. J., Hogan, T., Lynch, P., McLay, J., Reynolds, C. A., Sessions, W. R., Westphal, D. L., and Zhang, J.: Development of the Ensemble Navy Aerosol Analysis Prediction System (ENAAPS) and its application of the Data Assimilation Research Testbed (DART) in support of aerosol forecasting, Atmos. Chem. Phys., 16, 3927-3951, https://doi.org/10.5194/acp-16-3927-2016, 2016.

Salcedo, D., Onasch, T. B., Dzepina, K., Canagaratna, M. R., Zhang, Q., Huffman, J. A., Decarlo, P. F., Jayne, J. T., Mortimer, P., Worsnop, D. R., Kolb, C. E., Johnson, K. S., Zuberi, B., Marr, L. C., Volkamer, R., Molina, L. T., Molina, M. J., Cardenas, B., Bernabé, R. M., Márquez, C., Gaffney, J. S., Marley, N. A., Laskin, A., Shutthanandan, V., Xie, Y., Brune, W., Lesher, R., Shirley, T., and Jimenez, J. L.: Characterization of ambient aerosols in Mexico City during the MCMA-2003 campaign with Aerosol Mass Spectrometry: results from the CENICA Supersite, Atmospheric Chemistry and Physics, 6, 925-946, https://doi.org/10.5194/acp-6-925-2006, 2006.

Scarino, A. J., Obland, M. D., Fast, J. D., Burton, S. P., Ferrare, R. A., Hostetler, C. A., Berg, L. K., Lefer, B., Haman, C., Hair, J. W., Rogers, R. R., Butler, C., Cook, A. L., and Harper, D. B.: Comparison of mixed layer heights from airborne high spectral resolution lidar, ground-based measurements, and the WRF-Chem model during CalNex and CARES, Atmospheric Chemistry and Physics, 14, 5547-5560, https://doi.org/10.5194/acp-14-5547-2014, 2014.

Seibert, P.: Review and intercomparison of operational methods for the determination of the mixing height, Atmospheric Environment, 34, 1001-1027, https://doi.org/10.1016/s1352-2310(99)00349-0, 2000.

https://doi.org/10.5194/acp-2021-870
Preprint. Discussion started: 30 November 2021

Atmospheric Chemistry and Physics Discussions

1158 Seidel, D. J., Ao, C. O., and Li, K.: Estimating climatological planetary boundary layer heights
1159 from radiosonde observations: Comparison of methods and uncertainty analysis, Journal
1160 of Geophysical Research, 115, https://doi.org/10.1029/2009jd013680, 2010.
1161 Seinfeld, J. H. and Pandis, S. N.: Atmospheric Chemistry and Physics: From Air Pollution to
1162 Climate Change, Third, John Wiley & Sons, New York, 2016.
1163 Sessions, W. R., Reid, J. S., Benedetti, A., Colarco, P. R., da Silva, A., Lu, S., Sekiyama, T.,
1164 Tanaka, T. Y., Baldasano, J. M., Basart, S., Brooks, M. E., Eck, T. F., Iredell, M.,
1165 Hansen, J. A., Jorba, O. C., Juang, H. M. H., Lynch, P., Morcrette, J. J., Moorthi, S.,
1166 Mulcahy, J., Pradhan, Y., Razinger, M., Sampson, C. B., Wang, J., and Westphal, D. L.:
1167 Development towards a global operational aerosol consensus: basic climatological
1168 characteristics of the International Cooperative for Aerosol Prediction Multi-Model
1169 Ensemble (ICAP-MME), Atmos. Chem. Phys., 15, 335-362, https://doi.org/10.5194/acp-
1170 15-335-2015, 2015.
1171 Shi, Y., Zhang, J., Reid, J. S., Holben, B., Hyer, E. J., and Curtis, C.: An analysis of the
1172 collection 5 MODIS over-ocean aerosol optical depth product for its implication in
1173 aerosol assimilation, Atmospheric Chemistry and Physics, 11, 557-565,
1174 https://doi.org/10.5194/acp-11-557-2011, 2011.
1175 Shingler, T., Dey, S., Sorooshian, A., Brechtel, F. J., Wang, Z., Metcalf, A., Coggon, M.,
1176 Mülmenstädt, J., Russell, L. M., Jonsson, H. H., and Seinfeld, J. H.: Characterisation and
1177 airborne deployment of a new counterflow virtual impactor inlet, Atmospheric
1178 Measurement Techniques, 5, 1259-1269, https://doi.org/10.5194/amt-5-1259-2012, 2012.
1179 Shingler, T., Sorooshian, A., Ortega, A., Crosbie, E., Wonaschütz, A., Perring, A. E.,
1180 Beyersdorf, A., Ziemba, L., Jimenez, J. L., Campuzano-Jost, P., Mikoviny, T., Wisthaler,
1181 A., and Russell, L. M.: Ambient observations of hygroscopic growth factor and f (RH)
1182 below 1: Case studies from surface and airborne measurements, Journal of Geophysical
1183 Research: Atmospheres, 121, 13,661-613,677, https://doi.org/10.1002/2016jd025471,
1184 2016.
1185 Shinozuka, Y., Johnson, R. R., Flynn, C. J., Russell, P. B., Schmid, B., Redemann, J., Dunagan,
1186 S. E., Kluzek, C. D., Hubbe, J. M., Segal-Rosenheimer, M., Livingston, J. M., Eck, T. F.,
1187 Wagener, R., Gregory, L., Chand, D., Berg, L. K., Rogers, R. R., Ferrare, R. A., Hair, J.
1188 W., Hostetler, C. A., and Burton, S. P.: Hyperspectral aerosol optical depths from TCAP
1189 flights, Journal of Geophysical Research: Atmospheres, 118, 12,180-112,194,
1190 https://doi.org/10.1002/2013jd020596, 2013.
1191 Sobel, A. H., Camargo, S. J., Hall, T. M., Lee, C.-Y., Tippett, M. K., and Wing, A. A.: Human
1192 influence on tropical cyclone intensity, Science, 353, 242,
1193 https://doi.org/10.1126/science.aaf6574, 2016.
1194 Song, C., Woodcock, C. E., Seto, K. C., Lenney, M. P., and Macomber, S. A.: Classification and
1195 Change Detection Using Landsat TM Data, Remote Sensing of Environment, 75, 230-
1196 244, https://doi.org/10.1016/s0034-4257(00)00169-3, 2001.
1197 SPEC: SPEC FCDP Technical Manual (Rev.1.0 - Preliminary), 2013.
1198 SPEC: SPEC FCDP Technical Manual (Rev.2.0),
1199 http://www.specinc.com/sites/default/files/software_and_manuals/, 2019.
1200 Stahl, C., Cruz, M. T., Bañaga, P. A., Betito, G., Braun, R. A., Aghdam, M. A., Cambaliza, M.
1201 O., Lorenzo, G. R., Macdonald, A. B., Hilario, M. R. A., Pabroa, P. C., Yee, J. R.,
1202 Simpas, J. B., and Sorooshian, A.: Sources and characteristics of size-resolved particulate
1203 organic acids and methanesulfonate in a coastal megacity: Manila, Philippines,

Atmospheric Chemistry and Physics, 20, 15907-15935, https://doi.org/10.5194/acp-20-15907-2020, 2020.

Stull, R. B.: An Introduction to Boundary Layer Meteorology, Springer Science & Business Media1988.

Sun, Y., Solomon, S., Dai, A., and Portmann, R. W.: How Often Will It Rain?, Journal of Climate, 20, 4801-4818, https://doi.org/10.1175/jcli4263.1, 2007.

Takegawa, N., Miyazaki, Y., Kondo, Y., Komazaki, Y., Miyakawa, T., Jimenez, J. L., Jayne, J. T., Worsnop, D. R., Allan, J. D., and Weber, R. J.: Characterization of an Aerodyne Aerosol Mass Spectrometer (AMS): Intercomparison with Other Aerosol Instruments, Aerosol Science and Technology, 39, 760-770, https://doi.org/10.1080/02786820500243404, 2005.

Thornton, J. A., Virts, K. S., Holzworth, R. H., and Mitchell, T. P.: Lightning enhancement over major oceanic shipping lanes, Geophysical Research Letters, 44, 9102-9111, https://doi.org/10.1002/2017gl074982, 2017.

Titos, G., Cazorla, A., Zieger, P., Andrews, E., Lyamani, H., Granados-Muñoz, M. J., Olmo, F. J., and Alados-Arboledas, L.: Effect of hygroscopic growth on the aerosol light-scattering coefficient: A review of measurements, techniques and error sources, Atmospheric Environment, 141, 494-507, https://doi.org/10.1016/j.atmosenv.2016.07.021, 2016.

Vaisala: Dropsonde RD41, RD41 datasheet, https://www.vaisala.com/sites/default/files/documents/RD41-Datasheet-B211706EN.pdf, 2020.

Wang, Z., Sorooshian, A., Prabhakar, G., Coggon, M. M., and Jonsson, H. H.: Impact of emissions from shipping, land, and the ocean on stratocumulus cloud water elemental composition during the 2011 E-PEACE field campaign, Atmospheric Environment, 89, 570-580, https://doi.org/10.1016/j.atmosenv.2014.01.020, 2014.

Xian, P., Reid, J. S., Turk, J. F., Hyer, E. J., and Westphal, D. L.: Impact of modeled versus satellite measured tropical precipitation on regional smoke optical thickness in an aerosol transport model, Geophysical Research Letters, 36, https://doi.org/10.1029/2009gl038823, 2009.

Xian, P., Reid, J. S., Atwood, S. A., Johnson, R. S., Hyer, E. J., Westphal, D. L., and Sessions, W.: Smoke aerosol transport patterns over the Maritime Continent, Atmospheric Research, 122, 469-485, https://doi.org/10.1016/j.atmosres.2012.05.006, 2013.

Yumimoto, K., Tanaka, T. Y., Oshima, N., and Maki, T.: JRAero: the Japanese Reanalysis for Aerosol v1.0, Geoscientific Model Development, 10, 3225-3253, https://doi.org/10.5194/gmd-10-3225-2017, 2017.

Yusuf, A. A. and Francisco, H.: Climate change vulnerability mapping for Southeast Asia, Economy and Environment Program for Southeast Asia (EEPSEA) report, available at: http://www.eepsea.net, 1-26, 2009.

Zhang, J. and Reid, J. S.: MODIS aerosol product analysis for data assimilation: Assessment of over-ocean level 2 aerosol optical thickness retrievals, Journal of Geophysical Research, 111, https://doi.org/10.1029/2005jd006898, 2006.

Zhang, J., Reid, J. S., Westphal, D. L., Baker, N. L., and Hyer, E. J.: A system for operational aerosol optical depth data assimilation over global oceans, Journal of Geophysical Research: Atmospheres, 113, https://doi.org/10.1029/2007JD009065, 2008.

Zhu, J., Xia, X., Wang, J., Che, H., Chen, H., Zhang, J., Xu, X., Levy, R., Oo, M., Holz, R., and Ayoub, M.: Evaluation of Aerosol Optical Depth and Aerosol Models from VIIRS

https://doi.org/10.5194/acp-2021-870
Preprint. Discussion started: 30 November 2021

Retrieval Algorithms over North China Plain, Remote Sensing, 9, 432, https://doi.org/10.3390/rs9050432, 2017.

Zhu, X., Tang, G., Guo, J., Hu, B., Song, T., Wang, L., Xin, J., Gao, W., Münkel, C., Schäfer, K., Li, X., and Wang, Y.: Mixing layer height on the North China Plain and meteorological evidence of serious air pollution in southern Hebei, Atmospheric Chemistry and Physics, 18, 4897-4910, https://doi.org/10.5194/acp-18-4897-2018, 2018.

Ziemba, L. D., Lee Thornhill, K., Ferrare, R., Barrick, J., Beyersdorf, A. J., Chen, G., Crumeyrolle, S. N., Hair, J., Hostetler, C., Hudgins, C., Obland, M., Rogers, R., Scarino, A. J., Winstead, E. L., and Anderson, B. E.: Airborne observations of aerosol extinction by in situ and remote-sensing techniques: Evaluation of particle hygroscopicity, Geophysical Research Letters, 40, 417-422, https://doi.org.10.1029/2012gl054428, 2013.